TITLE

Evolution of connectivity architecture in the *Drosophila* mushroom body

AUTHORS

Kaitlyn Elizabeth Ellis[1], Hayley Smihula[1], Ishani Ganguly[2], Eva Vigato[1], Sven Bervoets[1], Thomas O. Auer[3], Richard Benton[3], Ashok Litwin-Kumar[2] and Sophie Jeanne Cécile Caron[1,*]

AFFILIATIONS

[1]School of Biological Sciences, University of Utah, Salt Lake City, United States.
[2]Center for Theoretical Neuroscience, Columbia University, New York, United States.
[3]Center for Integrative Genomics, Faculty of Biology and Medicine, University of Lausanne, Lausanne, Switzerland
[*]Correspondence: sophie.caron@utah.edu

ABSTRACT

Brain evolution has primarily been studied at the macroscopic level by comparing the relative size of homologous brain centers between species. How neuronal circuits change at the cellular level over evolutionary time remains largely unanswered. Here, using a phylogenetically informed framework, we compare the olfactory circuits of three closely related *Drosophila* species that differ radically in their chemical ecology: the generalists *Drosophila melanogaster* and *Drosophila simulans* that feed on fermenting fruit, and *Drosophila sechellia* that specializes on ripe noni fruit. We examine a central part of the olfactory circuit that has not yet been investigated in these species — the connections between the projection neurons of the antennal lobe and the Kenyon cells of the mushroom body, an associative brain center — to identify species-specific connectivity patterns. We found that neurons encoding food odors — the DC3 neurons in *D. melanogaster* and *D. simulans* and the DL2d neurons in *D. sechellia* — connect more frequently with Kenyon cells, giving rise to species-specific biases in connectivity. These species-specific differences in connectivity reflect two distinct neuronal phenotypes: in the number of projection neurons or in the number of presynaptic boutons formed by individual projection neurons. Our study shows how

fine-grained aspects of connectivity architecture in a higher brain center can change during evolution to reflect the chemical ecology of a species.

MAIN TEXT

Brain evolution has been primarily studied at the macroscopic level by comparing gross neuroanatomical features in homologous brain centers across distantly related species[1–3]. This pioneering work revealed that, over intermediate evolutionary timescales, the number of specialized brain centers does not change considerably, but the types and number of neurons forming these centers can vary greatly. Recent advances in comparative transcriptomics have provided new insights into the evolution and diversification of neurons, revealing how subtle variations in highly conserved regulatory gene networks can give rise to drastic changes in the rate at which neuronal progenitors proliferate or the types of neuron they give rise to[4]. To what degree such changes reflect evolutionary pressures remains unclear. Moreover, how such changes manifest themselves at the level of neuronal circuits is not yet understood, as it remains technically challenging to delineate neuronal circuits in non-traditional model systems and to compare them across species with different evolutionary trajectories[5].

Flies in the genus *Drosophila* have evolved to exploit a remarkable diversity of ecological niches[6]. The phylogeny of most *Drosophila* species has been resolved, revealing that even closely related *Drosophila* species can inhabit drastically different environments[7]. For instance, *Drosophila sechellia*, a species endemic to the Seychelles islands, is a specialist for noni — a toxic fruit that produces a distinctive bouquet of pungent acids — whereas its closest relative, *Drosophila simulans*, is a generalist and a human commensal that can be found in most cosmopolitan areas[8–11] (Figure 1a). A mere 0.25 million years of evolution separate these two species from their common ancestor, and only 3 million years separate their common ancestor from their well-studied relative, *Drosophila melanogaster*[7]. *D. melanogaster* is also a human commensal whose ecology largely overlaps with that of *D. simulans*[12]. These inverse relationships — phylogenetically, *D. sechellia* is closer to *D. simulans* while ecologically *D. melanogaster and D. simulans* are more alike — make this group of *Drosophila* highly suitable for investigating how neuronal circuits evolve over comparatively short timescales.

Olfactory driven behaviors used to locate food sources are most likely one of the most important ways whereby a species can adapt to its ecological niche. In *D. melanogaster,* most

olfactory sensory neurons express only one receptor gene, and the axons of neurons expressing the same receptor gene(s) converge on a specific glomerulus in the antennal lobe, forming a stereotypical map[13,14] (Figure 1b). The genomes of *D. melanogaster*, *D. simulans* and *D. sechellia* harbor a comparable number of functional olfactory receptor genes, and homologous glomeruli can be identified in the antennal lobe in these species[15,16]. In *D. sechellia*, however, a few olfactory sensory neurons show species-specific responses to noni odors: Or22a-expressing neurons are preferentially activated by methyl esters whereas Ir75b-expressing neurons are most sensitive to hexanoic acid[16–20]. In *D. melanogaster,* Or22a-expressing neurons are broadly tuned to different ethyl esters whereas Ir75b-expressing neurons are broadly tuned to shorter-chain acids[16–20]. These species-specific tuning properties are due to specific amino acid differences in the presumed ligand-binding domain of Or22a and Ir75b receptors[16,20]. In addition, there are two- to three-fold more Or22a- and Ir75b-expressing neurons in *D. sechellia*, and the glomeruli innervated by these neurons, DM2 and DL2d, respectively, are larger[16–18]. Other glomeruli — such as VM5d, which is innervated by Or85c/b-expressing neurons — are also larger in *D. sechellia* compared to *D. melanogaster*[16,18,19]

Whether and how the changes that occurred at the levels of receptor proteins and sensory neurons are reflected downstream, at the level of higher processing centers, is largely unknown. Projection neurons innervating individual antennal lobe glomeruli relay olfactory information to the mushroom body, an associative brain center, and the lateral horn, a center that mediates innate responses to odors[21] (Figure 1b). The projection neurons of the antennal lobe and the Kenyon cells of the mushroom body have been studied in detail in *D. melanogaster*. Each glomerulus type is innervated by a distinct, but largely stereotyped number of projection neurons, from one up to eight[22]. The mushroom body consists of about 2,000 neurons, called 'Kenyon cells', that can be divided into three major types (α/β, α'/β' and γ Kenyon cells); each Kenyon cell receives input from a small number of projection neurons, on average seven[23,24]. The connectivity architecture between projection neurons and Kenyon cells has been resolved, revealing two important principles: first, these connections are unstructured, in that individual Kenyon cells integrate inputs from a random set of projection neurons; second, some types of projection neuron connect more frequently to Kenyon cells than others, leading to a biased representation of glomeruli in the mushroom body[24–27]. These two connectivity patterns — randomization of input and biased connectivity — are genetically hardwired, suggesting that they might be shaped by evolutionary pressures[28].

RESULTS

Randomization of input is conserved across *Drosophila* species

105 To compare features of the connectivity architecture between projection neurons and Kenyon cells in *D. melanogaster*, *D. simulans* and *D. sechellia*, we first resolved gross anatomical features of the antennal lobes of these species. Using confocal images of brains immuno-stained with a neuropil marker, we reconstructed entire antennal lobes by manually tracing the borders of individual glomeruli on single planes and projecting their volumes in three-dimensional space
110 (Extended Data Figure 1). The resulting projections preserved the shape, volume and location of all the glomeruli forming an antennal lobe. Each glomerulus was annotated using the well-characterized *D. melanogaster* antennal lobe map, which was generated using similar methods, as a reference[13,14,29]. Glomerular volumes were compared across species (Extended Data Table 1). We found that the antennal lobe map is largely conserved in the three species and contains a
115 total of 51 glomeruli that can be recognized based on their shape and location. The volumes of most glomeruli are comparable across species with a few exceptions, including the noni-responsive DL2d, DM2 and VM5d glomeruli, which are larger in *D. sechellia*, as previously reported (DL2d: *D. melanogaster*: 1565 $\pm$ 334 μm^3 (n = 3); *D. simulans*: 2007 $\pm$ 185 μm^3 (n = 3); *D. sechellia*: 3066 $\pm$ 296 μm^3 (n = 3); DM2: *D. melanogaster*: 3139 $\pm$ 227 μm^3 (n = 3); *D.*
120 *simulans*: 3169 $\pm$ 227 μm^3 (n = 3); *D. sechellia*: 4594 $\pm$ 127 μm^3 (n = 3); VM5d: *D. melanogaster*: 905 $\pm$ 115 μm^3 (n = 3); *D. simulans*: 1773 $\pm$ 127 μm^3 (n = 3); *D. sechellia*: 3793 $\pm$ 153 μm^3 (n = 3))[16,18-20]. Despite these volume differences, the antennal lobes of the three species investigated are macroscopically nearly identical, which is in line with the notion that gross anatomy is conserved over the fairly short evolutionary distances separating the three species.

125

We next set out to compare the global connectivity architecture of the mushroom body across the three species by adapting the technique we previously developed to map projection neuron–Kenyon cell connections in *D. melanogaster*[25]. For each species, individual Kenyon cells were photo-labeled in flies carrying the broad neuronal driver *nSynaptobrevin-GAL4* and a *UAS-*
130 *photoactivatable-GFP* effector transgene. In *D. melanogaster*, there are three major types of Kenyon cell — α/β, α'/β' and γ Kenyon cells — and Kenyon cells from each type form a variable number of claw-shaped dendritic terminals. α/β, α'/β' and γ Kenyon cells were found in all three species, appear morphologically indistinguishable from one another and form on average a comparable number of claw-shaped dendritic terminals[23] (Extended Data Figure 2). To identify

135 the projection neurons connected to a photo-labeled Kenyon cell, a red-dye was electroporated sequentially in most of the claw-shaped dendritic terminals formed by that cell (Figure 1c, Extended Data Figure 3). Using this technique, the inputs of hundreds of Kenyon cells were identified in terms of the glomeruli from which they originate. We reported these results in a connectivity matrix that summarizes the glomerular inputs to 200 Kenyon cells. Statistical
140 analyses of the resulting matrix can be used to reveal structured patterns of connectivity, such as whether groups of glomeruli are preferentially connected to the same Kenyon cells or whether projection neuron–Kenyon cell connections are random and biased[25,28]. We generated a total of four such connectivity matrices (Figure 1d): two using *D. melanogaster* males and females (a total of 687 and 704 connections, respectively), one using *D. simulans* females (717 connections) and
145 one using *D. sechellia* females (692 connections).

We performed an unbiased search for potential structural features in these connectivity matrices using principal component analysis. The variance associated with individual principal component projections provides a sensitive measure of structure as we have previously
150 shown[25,28]. We extracted correlations within a given experimental connectivity matrix and compared them to correlations extracted from matrices in which connections were randomly shuffled. In these shuffled matrices, the total number of connections between projection neurons and Kenyon cells is the same as the number of connections reported in each experimental matrix, but the connections were randomly assigned ('uniform shuffle matrices'). We also generated a
155 second set of shuffle matrices in which the connections were scrambled but the frequencies at which projection neurons from each glomerulus connect to Kenyon cells were fixed to reflect the frequencies measured experimentally ('biased shuffle matrices'). We found that the observed spectrum of variances is not significantly different to that of the biased shuffle matrices, but does significantly deviate from that of the uniform shuffle matrices (Figure 2a,b). These results suggest
160 that there are no detectable structural features in the experimental matrices other than the structure generated by the biases in connectivity frequencies.

Biases in connectivity correlate with the chemical ecology of a species

165 If the connections between projection neurons and Kenyon cells were completely random, we would expect Kenyon cells to integrate input uniformly across glomeruli, and each glomerulus to have a connectivity frequency of about 2%. Yet, we found that the connections between projection neurons and Kenyon cells are biased: some glomeruli are overrepresented and have a

connectivity frequency significantly higher than 2%, whereas some glomeruli are underrepresented and have a connectivity frequency significantly lower than 2% (Extended Data Figure 4). The result is a non-uniform distribution of connectivity frequencies. We found that there are between nine and 12 overrepresented glomeruli (glomeruli with connectivity frequencies higher than 2%, p-value < 0.05) and between 10 and 13 underrepresented glomeruli (glomeruli with connectivity frequencies lower than 2%, p-value < 0.05) within each connectivity matrix. This result shows that the non-uniform distribution of connectivity frequencies is a feature present across species.

To compare the overall extent of bias in the distributions of connectivity frequencies derived from the connectivity matrices, we inferred their Jensen-Shannon distances. This statistical method measures the similarity of two probability distributions, with a distance of zero indicating identical distributions. To gauge the extent to which the Jensen-Shannon distance indicates overall similarity of the observed distributions in connectivity frequencies, we compared the distributions of connectivity frequencies measured in the experimental matrices to those measured using the corresponding uniform shuffle matrices and obtained distances ranging from 0.23 to 0.27; when we compared the distributions of connectivity frequencies measured in the experimental matrices to those measured using the biased shuffle matrices, we obtained distances ranging from 0.08 to 0.09 (Extended Data Figure 5). When we compared the distributions of connectivity frequencies measured using two *D. melanogaster* female matrices — one matrix was generated in this study and the other was generated in a previous study[28] — we obtained a relatively short distance of 0.17 (Figure 2c). Likewise, we obtained a relatively short distance of 0.15 when we compared the distributions measured in *D. melanogaster* females and males. This result suggests that the biases in connectivity are largely similar in both sexes. The distances measured when comparing *D. melanogaster* and *D. simulans* range from 0.16 to 0.17, indicating that the overall extent of bias in connectivity is similar in these species. By contrast, the distances between *D. melanogaster* and *D. sechellia* range from 0.20 to 0.22, whereas the distance between *D. simulans* and *D. sechellia* is 0.24, showing that the overall extent of biases in connectivity is higher in *D. sechellia* than in its sibling species. As *D. sechellia* and *D. simulans* are phylogenetically more closely related to each other than to *D. melanogaster*, the observed pattern suggests that the overall similarity in biases is not a function of evolutionary relatedness.

We next investigated whether the larger Jensen-Shannon distances measured for *D. sechellia* result from small differences in connectivity frequencies distributed across glomeruli or

whether they result from large differences restricted to a few glomeruli. We performed pairwise comparisons and measured the ratio of connectivity frequencies obtained for a given glomerulus in two different matrices (connectivity frequency measured in matrix 1 divided by the connectivity frequency measured in matrix 2) (Figure 2d). We found that most glomeruli are connected to Kenyon cells at similar frequencies in the six possible pairwise comparisons but that nine glomeruli are connected at significantly different frequencies in at least one pairwise comparison (p-value < 0.01; Benjamini-Hochberg procedure with false discovery rate of 0.10, see Extended Data Table 2 for exact p-values). This result indicates that significant changes in only a fraction of the glomeruli account for the observed shift in biases between the three species.

In only one of the nine cases, the change concerned *D. simulans*, where the VL2a glomerulus was found to be connected at lower frequency than in *D. melanogaster* (VL2a connectivity frequencies: *D. simulans*: 1.36%, *D. melanogaster*: 4.21%, p-value = 0.002068546, *D. sechellia*: 3.34%, p-value = 0.044418781). In all other cases, the significant changes occurred in *D. sechellia*. Two glomeruli — DL2d and DP1l, which receive input from the acid-sensing Ir75b- and Ir75a-expressing neurons, respectively — were found to be connected at higher frequencies in *D. sechellia* than in one of the other two species (DL2d connectivity frequencies: *D. sechellia*: 3.19%, *D. simulans*: 0.68%, p-value = 0.002030026, *D. melanogaster*: 1.02%, p-value = 0.010694533; DP1l: *D. sechellia*: 3.19%, *D. melanogaster*: 0.44%, p-value = 0.000213936, *D. simulans*: 0.95%, p-value = 0.010694533). Six glomeruli — namely the DC3, VA1d, VA7m, VC3, VC4 and VM5v glomeruli — were connected at lower frequencies in *D. sechellia* than in one one or both species. Four of these glomeruli receive input from olfactory sensory neurons tuned to various fruit volatiles: the Or83c-expressing neurons associated with the DC3 glomerulus are narrowly tuned to farnesol, a citrus odor, whereas the neurons associated with the VC3 (Or35a-expressing neurons), VC4 (Or67c-expressing neurons) and VM5v (Or98a-expressing neurons) glomeruli are broadly tuned to alcohols and esters produced by fermenting fruits[13,14,30–32] (connectivity frequencies: DC3: *D. sechellia*: 1.37%, *D. melanogaster*: 4.50%, p-value = 0.000105671, *D. simulans*: 4.91%, p-value = 6.18E-0.6; VC3: *D. sechellia*: 2.13%, *D. simulans*: 5.00%, p-value = 0.000724388, *D. melanogaster*: 2.90%, p-value = 0.0.282487997; VC4: *D. sechellia*: 0.61%, *D. simulans*: 2.46%, p-value = 0.044418781, *D. melanogaster*: 1.74%, p-value = 0.0.040115307; VM5v: *D. sechellia*: 1.82%, *D. simulans*: 5.05%, p-value = 5.83E-0.5, *D. melanogaster*: 3.36%, p-value = 0.016285553). The olfactory sensory neurons associated with the VA1d glomerulus (Or88a-expressing neurons) are tuned to methyl palmitate, a pheromone made by *D. melanogaster* females but not by *D. simulans* or *D. sechellia* females[33] (VA1d

connectivity frequencies: *D. sechellia*: 2.13%, *D. melanogaster*: 5.08%, *p*-value = 0.000724388, *D. simulans*: 3.14%, *p*-value = 0.0.087663066). The receptor identity and cognate odors of the olfactory sensory neurons that connect to the VA7m glomerulus remain to be identified.

240

Overall, these results show that species-specific differences in connectivity frequencies are restricted to a fraction of olfactory channels, which relay information about pheromones and food odors to the mushroom body, suggesting that the representation of specific channels changed as these species diverged. Most notably, in all but one case, the connectivity frequency
245 measured for a given glomerulus changes in the *D. sechellia* lineage, being more similar in *D. melanogaster* and *D. simulans* than when comparing any of these species to *D. sechellia*. As *D. sechellia* is more closely related to *D. simulans* than to *D. melanogaster*, this pattern appears not to be a function of phylogenetic relatedness, but instead of ecological relatedness. To better quantify this notion, we built a character matrix based on the connectivity frequencies measured
250 for each glomerulus. We derived a similarity tree for each glomerulus such that we could determine whether the resulting tree reflects phylogenetic relationships or whether it reflects ecological relationships. We found that 26 trees, as well as the tree generated using the entire character matrix, follow the ecological relationships and that only 12 trees follow the phylogenetics relationships (Figure 2e-g, Extended Data Figure 6). To contrast this finding, we also derived a
255 similarity tree using the coding sequence of the olfactory receptor(s) associated with a given glomerulus. Not surprisingly, we found that all these trees follow the phylogenetic relationships (Extended Data Figure 7). These observations show that changes in glomerular representation in the mushroom body are highly correlated with the ecology of a species, not its phylogeny, and, therefore, could have evolved in *D. sechellia* as this species diverged to exploit noni fruit.

260

Two morphological features of projection neurons underlie shifts in biases

From our analyses of the above data sets, we observed two types of change in the mushroom body connectivity architecture of *D. sechellia* when compared to that of *D. melanogaster* and *D.
265 simulans*: the representation of a few glomeruli either increases, for instance the representation of the DL2d and DP1l glomeruli, or decreases, for instance the representation of the DC3, VA1d, VA7m, VC3, VC4 and VM5v glomeruli. In *D. melanogaster*, it is known that biases in connectivity are a function of the overall number of presynaptic boutons formed in the mushroom body by the projection neurons associated with a given glomerulus[24,25,27]. Thus, changes in glomerular
270 representation across species could result from changes in the number of projection neurons

associated with a given glomerulus, changes in the number of presynaptic boutons individual projection neurons form or both. To determine whether any of these cases prevail, we photo-labeled (Figure 3a) and dye-labeled (Figure 4a) the projection neurons innervating a given glomerulus to quantify the number of neurons and measure the volume of the presynaptic boutons
275 the labeled neurons occupy in the mushroom body.

The DL2d and DP1l glomeruli are more frequently connected to Kenyon cells in *D. sechellia* (Figure 2d, Extended Data Table 2). We identified eight DL2d projection neurons in *D. sechellia* (five neurons located in the anterior-dorsal cluster, or adDL2d neurons, and three
280 neurons located in the ventral cluster, or vDL2d neurons) but only six DL2d projection neurons in *D. melanogaster* and *D. simulans* (five adDL2d neurons and one vDL2d neuron in both species) (Table 1, Figure 3b-c). The number of DL2d projection neurons identified in *D. melanogaster* is consistent with the number of projection neurons reported in the available connectomes of the *D. melanogaster* brain[22] (Extended Data Figure 8). In all species, the vDL2d neurons bypass the
285 mushroom body and project only to the lateral horn. Therefore, the number of neurons connecting the DL2d glomerulus to the mushroom body is the same in all species. However, collectively, the adDL2d neurons show larger bouton volume in *D. sechellia* than they do in the other species (bouton volume of all adDL2d neurons: *D. melanogaster*: 112.18 $\pm$ 12.41; *D. simulans*: 104.44 $\pm$ 25.93; *D. sechellia*: 348.29 $\pm$ 186.63; Table 1, Figure 3d). We found that the increased number of
290 connections between adDL2d neurons and Kenyon cells in *D. sechellia* is due to more presynaptic boutons being formed per neuron (Figure 4b-c, Extended Data Table 3). We also found that individual adDL2d neurons show more complex branching patterns based on several quantifiable parameters (Figure 4c, Extended Data Table 3). We identified a similar phenotype for the projection neurons associated with the DP1l glomerulus: there are three DP1l projection neurons
295 in *D. sechellia* (one neuron located in the lateral cluster, or lDP1l neuron, and two vDP1l neurons) but only two DP1l projection neurons in *D. melanogaster* (one lDP1l neuron and one vDP1l neuron) as it has been reported in the connectomes[22] (Table 1, Extended Data Figure 9). As with the vDL2d neurons, the vDP1l neurons bypass the mushroom body and only the lDP1l neurons connect to Kenyon cells. We found that for lDP1l neurons the bouton volume is larger in *D.
300 sechellia* than in *D. melanogaster* and *D. simulans* (bouton volume of the lDP1l neuron: *D. melanogaster*: 244.39 $\pm$ 69.00; *D. simulans*: 232.41 $\pm$ 100.73; *D. sechellia*: 388.91 $\pm$ 75.88).

The DC3 and VM5v glomeruli are less frequently connected to Kenyon cells in *D. sechellia* (Figure 2d, Extended Data Table 2). We identified two DC3 projection neurons in *D. sechellia* (two

305 adDC3 neurons) but as many as three in *D. melanogaster* (three adDC3 neurons as reported in the connectomes[22]) and six in *D. simulans* (three adDC3 neurons and three vDC3 neurons) (Table 1, Figure 3b-c, Extended Data Figure 8). In *D. simulans*, the vDC3 neurons bypass the mushroom body and project only to the lateral horn. The volume of presynaptic boutons collectively formed by the adDC3 neurons in the mushroom body is significantly smaller in *D. sechellia* than in *D.*
310 *melanogaster* and *D. simulans* (bouton volume of all adDC3 neurons: *D. melanogaster*: 370.15 ± 195.68; *D. simulans*: 364.06 ± 146.60; *D. sechellia*: 233.02 ± 83.80; Table 1, Figure 3d). However, individual adDC3 projection neurons are morphologically similar across species with no significant differences in branch length, number of forks or bouton number (bouton volume of individual adDC3 neuron: *D. melanogaster*: 184.15 ± 34.60; *D. simulans*: 169.01 ± 43.23; *D. sechellia*:
315 165.36 ± 25.56; Figure 4b-c, Extended Data Table 3). Thus, the decrease in the number of connections between adDC3 neurons and Kenyon cells in *D. sechellia* is due to a decrease in number of projection neurons innervating the DC3 glomerulus in that species. We identified a similar phenotype for the projection neurons associated with the VM5v glomerulus: there are two adVM5v projection neurons in *D. sechellia* but as many as three adVM5v projection neurons in
320 *D. melanogaster*, as reported in the connectomes[22], and three adVM5v projection neurons in *D. simulans* (Table 1, Figure 3b-c, Extended Data Figure 8). We found that, as for the adDC3 projection neurons, the adVM5v neurons form collectively a smaller bouton volume in *D. sechellia* but, individually, the VM5v neurons are similar across species (bouton volume of all VM5v neurons: *D. melanogaster*: 256.78 ± 104.09; *D. simulans*: 268.43 ± 132.67; *D. sechellia*: 140.14
325 ± 77.76; Table 1; bouton volume of individual VM5v neurons: *D. melanogaster*: 116.45 ± 18.68; *D. simulans*: 85.38 ± 17.48; *D. sechellia*: 169.73 ± 39.67; Figure 4b-c, Extended Data Table 3). Thus, as with the adDC3 neurons, there are fewer VM5v neurons in *D. sechellia*, and, therefore, fewer connections between the VM5v glomerulus and Kenyon cells. Combined with the observations made for the DL2d and DP1l projection neurons, these results suggest that
330 increases in glomerular representation in *D. sechellia* occur through increases in bouton number, whereas decreases in glomerular representation occur through decreases in the number of projection neurons associated with different glomeruli.

We did not detect significant interspecific differences for the VC3 and VL2a projection
335 neurons although we identified these glomeruli as differently represented in at least one of the species investigated (Table 1, Extended Data Figure 9). This result suggests that our photo-labeling and dye-labeling techniques might not be sensitive enough to detect all the morphological features — other than number of projection neurons and bouton volume — that underlie shifts in

connectivity. Alternatively, this result could reflect the relatively low stringency of the statistical tests used to identify significant shifts in connectivity frequencies — we used a false discovery rate of 0.10 — and it could suggest that these data points might be false positives. Although our photo-labeling and dye-labeling techniques might not fully capture the extent of morphological differences that exist between the species investigated, the interspecific differences they successfully identified seem specific and restricted to a small number of projection neurons. We have performed similar morphological analyses on neurons innervating glomeruli that we identified as identically represented in all three species, namely the DA2, DM2 and DP1m glomeruli. We could not detect any noticeable differences in the axonal termini that these projection neurons extend in the mushroom body (Table 1, Extended Data Figure 9).

Discussion

In this study, we harness a phylogenetically and ecologically informed approach to pinpoint evolutionary differences in neuronal connectivity architecture between three species of *Drosophila*. The species differ in the frequency with which inputs from a small set of olfactory channels — mainly those relaying information about food odors — are represented among the overall input to a higher-order processing center, the mushroom body. Notably, most of these differences are found in the specialist species *D. sechellia*, suggesting they are due to an ecological niche shift, rather than merely a function of phylogenetic distance. Evolutionary differences in sensory representation are caused by morphological alterations of the projection neurons connecting individual glomeruli to the mushroom body, either through changes in the number of projection neurons or through changes in the number of presynaptic boutons per neuron.

It is likely that other features of connectivity architecture underlie evolution of the mushroom body in *Drosophila* species. A recent electron microscopy-based study of the *D. melanogaster* mushroom body has revealed a subtle but significant connectivity pattern between a subgroup of projection neurons and the α/β and α′/β′ Kenyon cells, and our mapping technique may not be sensitive enough to capture these more subtle features of connectivity architecture[27,28]. Likewise, there are limitations regarding the forces driving the evolution of connectivity architecture in the mushroom body. For instance, it remains unclear whether the neuronal connectivity traits identified are variable in natural populations, especially those inhabiting in different environments. It remains equally unclear whether the changes that we

observed confer a fitness advantage and could be adaptive. The fact that we were able to correlate a visible neuronal phenotype with these connectivity changes, make such investigations theoretically possible in the future.

Evolutionary comparisons of the olfactory system in *Drosophila* species have so far mainly focused on peripheral components of the circuit, in particular the olfactory sensory neurons and the receptor genes they express[34]. What has remained less clear is whether changes in receptor cell response profile or amplitude are sufficient to lead to evolutionary shifts in chemosensory ecology or whether concomitant changes occur in higher brain centers. Our study provides the first evidence at the cellular level for such evolutionary changes in the connectivity architecture of higher olfactory brain centers. The fact that biases in connectivity are genetically encoded in *D. melanogaster*, and form independently of neuronal activity, indicates that the changes we uncovered are not merely a consequence of altered function at the periphery[28]. Instead, they represent an additional element of evolutionary change in circuit architecture and point to a locus in the central brain where evolution of neuronal circuits occurs.

How higher brain centers evolve remains, for the most part, completely unknown. Higher brain centers often feature more integrated circuits with many connections, and therefore it is conceivable that they might be less liable to change during evolution due to the disruptive impacts such changes might have across circuits. The changes we observed in this study are comparatively subtle, involving changes in the quantity of neuronal connections formed while leaving the overall random circuit architecture intact. Theoretical studies have demonstrated that randomization of input enables mushroom body-like networks to generate a representation space of high dimensionality, where many odors can be represented by non-overlapping neuronal ensembles[35–37]. We propose that biases in connectivity enable the mushroom body to better represent ecologically meaningful odors by increasing the coding space allocated to these odors, potentially increasing the fitness of an animal. Shifts in connectivity biases emphasize information streams that are most relevant to an animal without completely inactivating or adding *de novo* streams. This evolutionary pattern may be widespread across brain centers and species.

ACKNOWLEDGMENTS

We thank members of the Caron laboratory for comments on the manuscript; David Stern for sharing the *attp*^{2176} and *attp*^{2178} *D. simulans* strains and φC31 integrase mRNA; Vanessa Ruta for

sharing the *UAS-C3PA-GFP* plasmid; Adam Lin for preparation of the standard cornmeal agar medium; the Cell Imaging Core at the University of Utah for use of the Zeiss LSM 880 microscope; Ashley Platt and Miles Jacob for assistance with general laboratory concerns. This work has been funded by grants from the National Institute for Neurological Disorders and Stroke (R01 EB 029858, R01 NS 106018 and R01 NS 1079790), the National Science Foundation (DBI 1707398 and IOS 2042397), the Gatsby Charitable Foundation, the European Research Council (European Research Council Advanced Grant 833548) and the Swiss National Science Foundation (Ambizione Grant PZ00P3 185743). Further financial support was provided by the Eunice Kennedy Shriver National Institute of Child Health and Human Development (T32-HD-007491) (K.E.E.), the Department of Energy Computational Science Graduate Fellowship (DE-SC0022158) (I.G.), the Burroughs Wellcome Foundation (A.L.K.), the McKnight Endowment Fund (A.L.K.), the Simons Collaboration on the Global Brain (A.L.K.), the Human Frontier Science Program (LT000461/2015-L) (T.O.A.) and the Georges S. and Dolores Eccles Foundation (S.J.C.C.).

AUTHORS CONTRIBUTIONS

K.E.E. and S.J.C.C. conceived the project. H.M.S. generated and analyzed the antennal lobe reconstructions; K.E.E. photo-labeled projection neurons and Kenyon cells, dye-labeled individual projection neurons, and analyzed their morphology; K.E.E. generated the connectivity matrices; I.G. and A.L.K. performed the statistical analyses of the connectivity matrices; E.V. generated the similarity trees; S.B. performed crucial pilot experiments; T.O.A. and R.B. provided the *D. sechellia* transgenic lines and plasmids used to generate the *D. simulans* transgenes. K.E.E and S.J.C.C. wrote the manuscript with input from all other authors.

COMPETING INTERESTS DECLARATION

The authors declare no competing interests.

REFERENCES (MAIN TEXT)

1. Striedter, G. F. & Northcutt, R. G. *Brains Through Time*. (Oxford University Press, 2019). doi:10.1093/oso/9780195125689.001.0001.
2. Striedter, G. F. *Principles of brain evolution. Principles of brain evolution.* (Sinauer Associates, 2005).

3. Strausfeld. *Arthropod Brains*. (2011).
4. Tosches, M. A. From Cell Types to an Integrated Understanding of Brain Evolution: The Case of the Cerebral Cortex. *Annu Rev Cell Dev Biol* **37**, 495–517 (2021).
5. Roberts, R. J. v, Pop, S. & Prieto-Godino, L. L. Evolution of central neural circuits: state of the art and perspectives. *Nat Rev Neurosci* **23**, 725–743 (2022).
6. Markow, T. A. The secret lives of Drosophila flies. *Elife* **4**, (2015).
7. Drosophila 12 Genomes Consortium *et al.* Evolution of genes and genomes on the Drosophila phylogeny. *Nature* **450**, 203–18 (2007).
8. Sturtevant, A. H. A New Species Closely Resembling Drosophila Melanogaster. *Psyche (Camb Mass)* **26**, 153–155 (1919).
9. Tsacas, L. & Bächli, G. Drosophila sechellia. n. sp., huitieme espece du sous-groupe melanogaster des iles Seychelles (Diptera, Drosophilidae). *Rev. Fr. Entomol 3* 146–150 (1981).
10. R'Kha, S., Capy, P. & David, J. R. Host-plant specialization in the Drosophila melanogaster species complex: a physiological, behavioral, and genetical analysis. *Proceedings of the National Academy of Sciences* **88**, 1835–1839 (1991).
11. Auer, T. O., Shahandeh, M. P. & Benton, R. *Drosophila sechellia* : A Genetic Model for Behavioral Evolution and Neuroecology. *Annu Rev Genet* **55**, 527–554 (2021).
12. Lachaise, D. & Silvain, J.-F. How Two Afrotropical Endemics Made Two Cosmopolitan Human Commensals: the Drosophila Melanogaster–D. Simulans Palaeogeographic Riddle. *Genetica* **120**, 17–39 (2004).
13. Couto, A., Alenius, M. & Dickson, B. J. Molecular, anatomical, and functional organization of the Drosophila olfactory system. *Current Biology* **15**, 1535–1547 (2005).
14. Fishilevich, E. & Vosshall, L. B. Genetic and functional subdivision of the Drosophila antennal lobe. *Current Biology* **15**, 1548–1553 (2005).
15. McBride, C. S. & Arguello, J. R. Five Drosophila Genomes Reveal Nonneutral Evolution and the Signature of Host Specialization in the Chemoreceptor Superfamily. *Genetics* **177**, 1395–1416 (2007).
16. Auer, T. O. *et al.* Olfactory receptor and circuit evolution promote host specialization. *Nature* **579**, 402–408 (2020).
17. Stensmyr, M. C., Dekker, T. & Hansson, B. S. Evolution of the olfactory code in the *Drosophila melanogaster* subgroup. *Proc R Soc Lond B Biol Sci* **270**, 2333–2340 (2003).
18. Dekker, T., Ibba, I., Siju, K. P., Stensmyr, M. C. & Hansson, B. S. Olfactory shifts parallel superspecialism for toxic fruit in Drosophila melanogaster sibling, D. sechellia. *Current Biology* **16**, 101–109 (2006).
19. Ibba, I., Angioy, A. M., Hansson, B. S. & Dekker, T. Macroglomeruli for fruit odors change blend preference in Drosophila. *Naturwissenschaften* **97**, 1059–1066 (2010).
20. Prieto-Godino, L. L. *et al.* Evolution of Acid-Sensing Olfactory Circuits in Drosophilids. *Neuron* **93**, 661-676.e6 (2017).
21. Jefferis, G. S. X. E. *et al.* Comprehensive Maps of Drosophila Higher Olfactory Centers: Spatially Segregated Fruit and Pheromone Representation. *Cell* **128**, 1187–1203 (2007).
22. Schlegel, P. *et al.* Information flow, cell types and stereotypy in a full olfactory connectome. *Elife* **10**, (2021).

23. Aso, Y. *et al.* The neuronal architecture of the mushroom body provides a logic for associative learning. *Elife* **3**, (2014).
24. Li, F. *et al.* The connectome of the adult Drosophila mushroom body provides insights into function. *Elife* **9**, (2020).
25. Caron, S. J. C., Ruta, V., Abbott, L. F. & Axel, R. Random convergence of olfactory inputs in the Drosophila mushroom body. *Nature* **497**, 113–117 (2013).
26. Gruntman, E. & Turner, G. C. Integration of the olfactory code across dendritic claws of single mushroom body neurons. *Nat Neurosci* **16**, 1821–1829 (2013).
27. Zheng, Z. *et al.* Structured sampling of olfactory input by the fly mushroom body. *Current Biology* **32**, 3334-3349.e6 (2022).
28. Hayashi, T. T. *et al.* Mushroom body input connections form independently of sensory activity in Drosophila melanogaster. *Current Biology* **32**, 4000-4012.e5 (2022).
29. Grabe, V. *et al.* Elucidating the Neuronal Architecture of Olfactory Glomeruli in the Drosophila Antennal Lobe Resource Elucidating the Neuronal Architecture of Olfactory Glomeruli in the Drosophila Antennal Lobe. 3401–3413 (2016).
30. Hallem, E. A. & Carlson, J. R. Coding of Odors by a Receptor Repertoire. *Cell* **125**, 143–160 (2006).
31. Ronderos, D. S., Lin, C.-C., Potter, C. J. & Smith, D. P. Farnesol-Detecting Olfactory Neurons in Drosophila. *Journal of Neuroscience* **34**, 3959–3968 (2014).
32. Münch, D. & Galizia, C. G. DoOR 2.0 - Comprehensive Mapping of Drosophila melanogaster Odorant Responses. *Sci Rep* **6**, 21841 (2016).
33. Dweck, H. K. M. *et al.* Pheromones mediating copulation and attraction in *Drosophila*. *Proceedings of the National Academy of Sciences* **112**, (2015).
34. Zhao, Z. & McBride, C. S. Evolution of olfactory circuits in insects. *Journal of Comparative Physiology A* **206**, 353–367 (2020).
35. Luo, S. X., Axel, R. & Abbott, L. F. Generating sparse and selective third-order responses in the olfactory system of the fly. *Proceedings of the National Academy of Sciences* **107**, 10713–10718 (2010).
36. Stevens, C. F. What the fly's nose tells the fly's brain. *Proceedings of the National Academy of Sciences* **112**, 9460–9465 (2015).
37. Litwin-Kumar, A., Harris, K. D., Axel, R., Sompolinsky, H. & Abbott, L. F. Optimal Degrees of Synaptic Connectivity. *Neuron* **93**, 1153-1164.e7 (2017).
38. Stern, D. L. *et al.* Genetic and Transgenic Reagents for *Drosophila simulans* , *D. mauritiana* , *D. yakuba* , *D. santomea* , and *D. virilis*. *G3 Genes|Genomes|Genetics* **7**, 1339–1347 (2017).
39. Scheffer, L. K. *et al.* A connectome and analysis of the adult Drosophila central brain. *Elife* **9**, (2020).
40. Li, J., Ellis, K. E. & Caron, S. J. C. Photo-labeling neurons in the Drosophila brain. *STAR Protoc* **2**, 100381 (2021).
41. Ruta, V. *et al.* A dimorphic pheromone circuit in Drosophila from sensory input to descending output. *Nature* **468**, 686–690 (2010).
42. Schindelin, J. *et al.* Fiji: an open-source platform for biological-image analysis. *Nat Methods* **9**, 676–682 (2012).

43. Longair, M. H., Baker, D. A. & Armstrong, J. D. Simple Neurite Tracer: open source software for reconstruction, visualization and analysis of neuronal processes. *Bioinformatics* **27**, 2453–2454 (2011).
44. Wan, Y. *et al.* FluoRender: joint freehand segmentation and visualization for many-channel fluorescence data analysis. *BMC Bioinformatics* **18**, 280 (2017).
45. Goloboff, P. A., Farris, J. S. & Nixon, K. C. TNT, a free program for phylogenetic analysis. *Cladistics* **24**, 774–786 (2008).
46. Camacho, C. *et al.* BLAST+: architecture and applications. *BMC Bioinformatics* **10**, 421 (2009).
47. Souvorov, A. *et al.* Gnomon – NCBI eukaryotic gene prediction tool. Preprint at (2012).
48. Jones, D. T., Taylor, W. R. & Thornton, J. M. The rapid generation of mutation data matrices from protein sequences. *Bioinformatics* **8**, 275–282 (1992).
49. Edgar, R. C. MUSCLE: multiple sequence alignment with high accuracy and high throughput. *Nucleic Acids Res* **32**, 1792–1797 (2004).

Table 1 | Morphological features of photo-labeled projection neurons across species.

Projection neurons	Neuron number			Bouton cluster volume μm³		
	D. melanogaster	***D. simulans***	***D. sechellia***	***D. melanogaster***	***D. simulans***	***D. sechellia***
DA2	4 ± 0.80 lPNs	4 ± 1.02 lPNs	4 ± 0.40 lPNs	112.79 ± 11.30	110.95 ± 37.06	179.18 ± 31.76
DC3	3 ± 0.29 adPNs	3 adPNs, 3 vPNs	2 ± 0.29 adPNs	370.15 ± 195.68	364.06 ± 146.60	233.02 ± 83.80
DL2d	5 adPNs, 1 vPN	5 adPNs, 1 vPN	5 adPNs, 3 vPNs	112.18 ± 12.41	104.44 ± 25.93	348.29 ± 186.63
DM2	2 lPNs	2 lPNs	2 lPNs	367.38 ± 54.87	309.52 ± 89.42	365.40 ± 52.39
DP1l	1 lPN, 1 vPN	1 lPN, 2 vPNs	1 lPN, 2 vPNs	244.39 ± 69.00	232.41 ± 100.73	388.91 ± 75.88
DP1m	1 adPN	1 adPN	1 adPN	221.59 ± 72.28	172.85 ± 113.80	260.95 ± 105.19
VA1d	3 adPNs, 1 vPN	3 adPNs, 1 vPN	3 ± 0.40 adPNs, 1 vPN	205.89 ± 26.65	195.78 ± 109.79	155.87 ± 50.25
VC3	3 adPNs	3 adPNs	3 adPNs	200.70 ± 97.03	158.48 ± 90.40	143.59 ± 46.17
VL2a	1 adPN, 3 vPNs	1 adPN, 3 vPNs	1 adPN, 3 vPNs	174.36 ± 64.22	156.05 ± 79.93	208.92 ± 60.55
VM5v	3 ± 0.49 adPNs	3 ± 0.40 adPNs	2 ± 0.33 adPNs	256.78 ± 104.09	268.43 ± 132.67	140.14 ± 77.76

Table 1. Morphological features of photo-labeled projection neurons across species. Morphological features of projection neurons — namely the number of neurons associated with a given glomerulus and the volume of the presynaptic sites these neurons form in the mushroom
565 body — were measured and compared across species (*n* = 5 for each type of projection neuron). Projection neurons showing significant shifts in connectivity frequencies (DC3, DL2d, VM5v, DP1l, VA1d, VC3, and VL2a projection neurons) were analyzed as well as some projection neurons that did not show significant shifts in connectivity frequencies (DA2, DM2, and DP1m projection neurons). Projection neurons were typed based on whether their cell bodies are located in the
570 anterior-dorsal (ad), lateral (l) or ventral cluster (v).

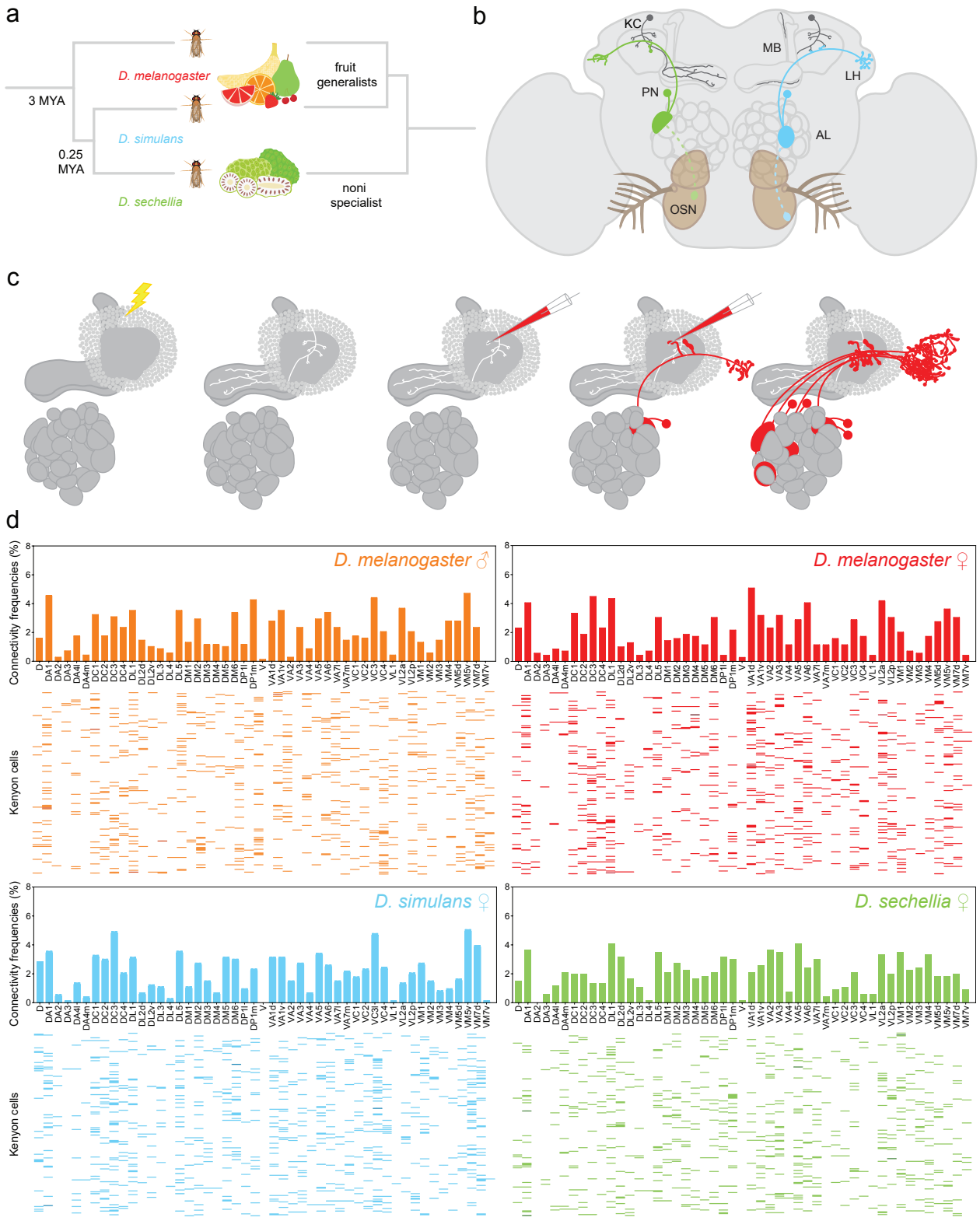
a
3 MYA
0.25 MYA
D. melanogaster
D. simulans
D. sechellia
fruit generalists
noni specialist
b
KC
MB
LH
PN
AL
OSN
c
d
D. melanogaster ♂
D. melanogaster ♀
D. simulans ♀
D. sechellia ♀
Connectivity frequencies (%)
Kenyon cells

Figure 1

Figure 1. Mapping Kenyon cell inputs in *Drosophila* species living in different ecological
575 **niches.** (a) Schematic depicting the phylogenetic relationships of *D. melanogaster* (red), *D. simulans* (blue), and *D. sechellia* (green) on the left and their ecological relationships on the right. (b) Schematic depicting the *Drosophila* olfactory circuit: olfactory sensory neurons that express the same receptor gene(s) (OSNs, green and blue neurons with dotted outline) converge onto the same glomerulus in the antennal lobe (AL); projection neurons (PNs, green and blue neurons with
580 full outline) connect individual glomeruli to the mushroom body (MB) and the lateral horn (LH). Kenyon cells (dark grey) receive input from a small number of projection neurons. (c) Schematic depicting the technique used to map connections between projection neurons and Kenyon cells: a Kenyon cell is photo-labelled (white) and the projection neurons connected to each of its claw are dye-labeled (red) such that the antennal lobe glomeruli innervated by the labeled projection
585 neurons can be identified; see Extended Figure 3 for a more detailed description of the technique. (d) Connections between glomeruli and Kenyon cells were mapped in *D. melanogaster*, *D. simulans* and *D. sechellia*, and all connections are reported in four connectivity matrices (*D. melanogaster* males: top left panel and orange (687 connections); *D. melanogaster* females: top right panel and red (704 connections); *D. simulans* females: bottom left panel and blue (717
590 connections); *D. sechellia* females: bottom right panel and green (692 connections)). In each matrix, a row corresponds to a Kenyon cell — there are 200 Kenyon cells per matrix — and each column corresponds to the different antennal lobe glomeruli; each colored bar indicates the input connections of a given Kenyon cell, and the intensity of the color denotes the number of connections found between a particular Kenyon cell and a given glomerulus (light: one
595 connection; medium: two connections; dark: three connections). The bar graphs above the matrices represent the frequencies at which a particular glomerulus was connected to Kenyon cells as measured in a given matrix.

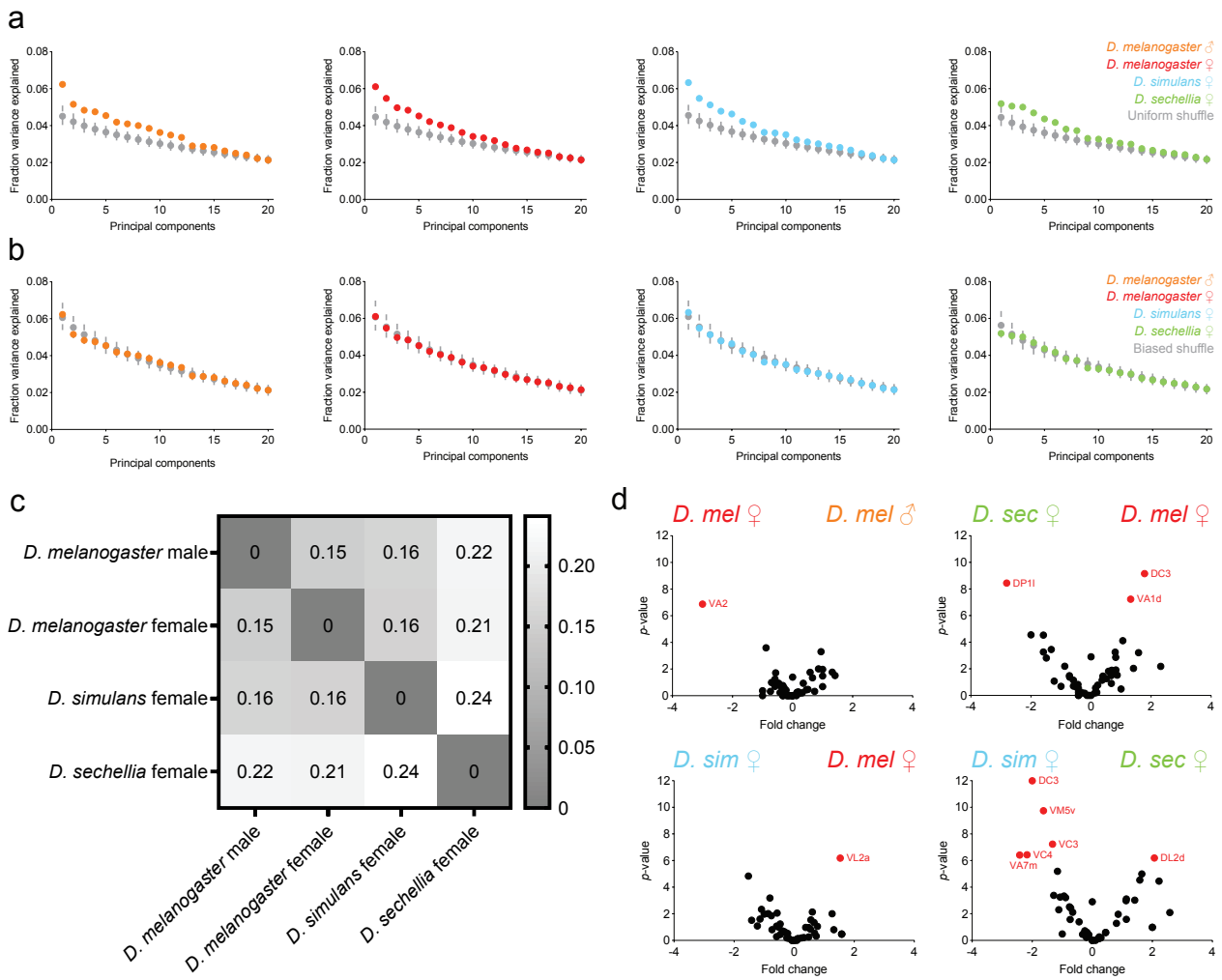

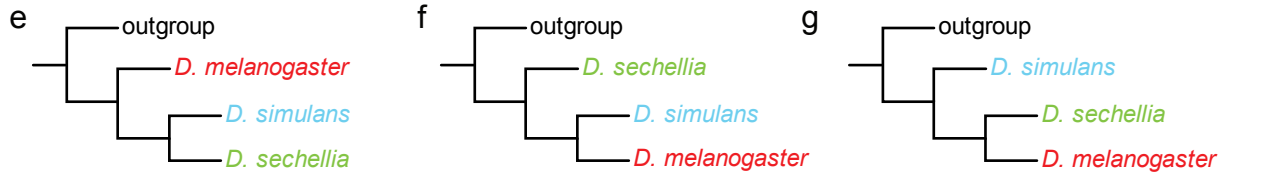

DA2, DA4l, DL4, DL5, DM2, DM4, DP1m, V, VA4, VA5, VM1, VM5d

D, DA3, DA4m, DC1, DC3, DC4, DL2d, DL2v,DM1, DM3, DM6, DP1l, VA1d, VA1v, VA6,VA7l, VC3, VL1, VL2p, VM2, VM3, VM4, VM5v,VM7d, VM7v

DA1, DC2, DL1, DL3, DM5, VA2, VA3, VA7m, VC1, VC2, VC4, VL2a

Figure 2

Figure 2. Shifts in connectivity biases across *Drosophila* species. (a-b) Principal components were extracted using each connectivity matrix as well as their uniform shuffle versions (a) or biased shuffle versions (b); the fraction of the variance explained by each component was measured (*D. melanogaster* males: far left panels and orange; *D. melanogaster* females: middle left panels and red; *D. simulans* females: middle right panels and blue; *D. sechellia* females: far right panels and green; colored circles: experimental matrices, grey circles: fixed-shuffle matrices); error bars represent 95% confidence interval. (c) The Jensen-Shannon distances were measured by comparing the distributions in connectivity frequencies observed experimentally and reported as a heat map; the color bar denotes the length of the distances measured. See Extended Data Figure 5 for the complete set of Jensen-Shannon distances including those measured when comparing the experimental matrices to their shuffle versions or when comparing the experimental matrices to an experimental matrix obtained in a previous study[28]. (d) The p-value measured for each type of projection neuron was plotted against the $\log_2$ fold change measured when comparing the connectivity frequencies measured for that type of projection neuron in the two matrices indicated on the plot. The statistical significance, or 'p-value', was measured for each type of projection neuron using the Fisher's exact test; to control for false positives, p-values were adjusted with a false discovery rate of 0.10 using a Benjamini-Hochberg procedure. Within these plots, a fold change with a value of 0 indicates that there is no shift in frequencies between the two matrices, whereas a fold change that is smaller or greater than 0 indicates that a given type of projection neuron connects more frequently in one matrix than the other. Data points with p-values smaller than 0.01 are identified with a label (red circles); all other data points have p-values greater than 0.01 (black circles). (e-g) Similarity trees were generated using the Tree analysis Using New Technology (TNT) software. Trait used was the connectivity frequency measured for a given glomerulus in a given species (e-g) Trees generated for individual glomeruli were found to either follow the known phylogenetic relationships (e), the ecological relationships (f) or neither (g). See Extended Data Figure 6 for individual trees and more detailed explanations of the analyses.

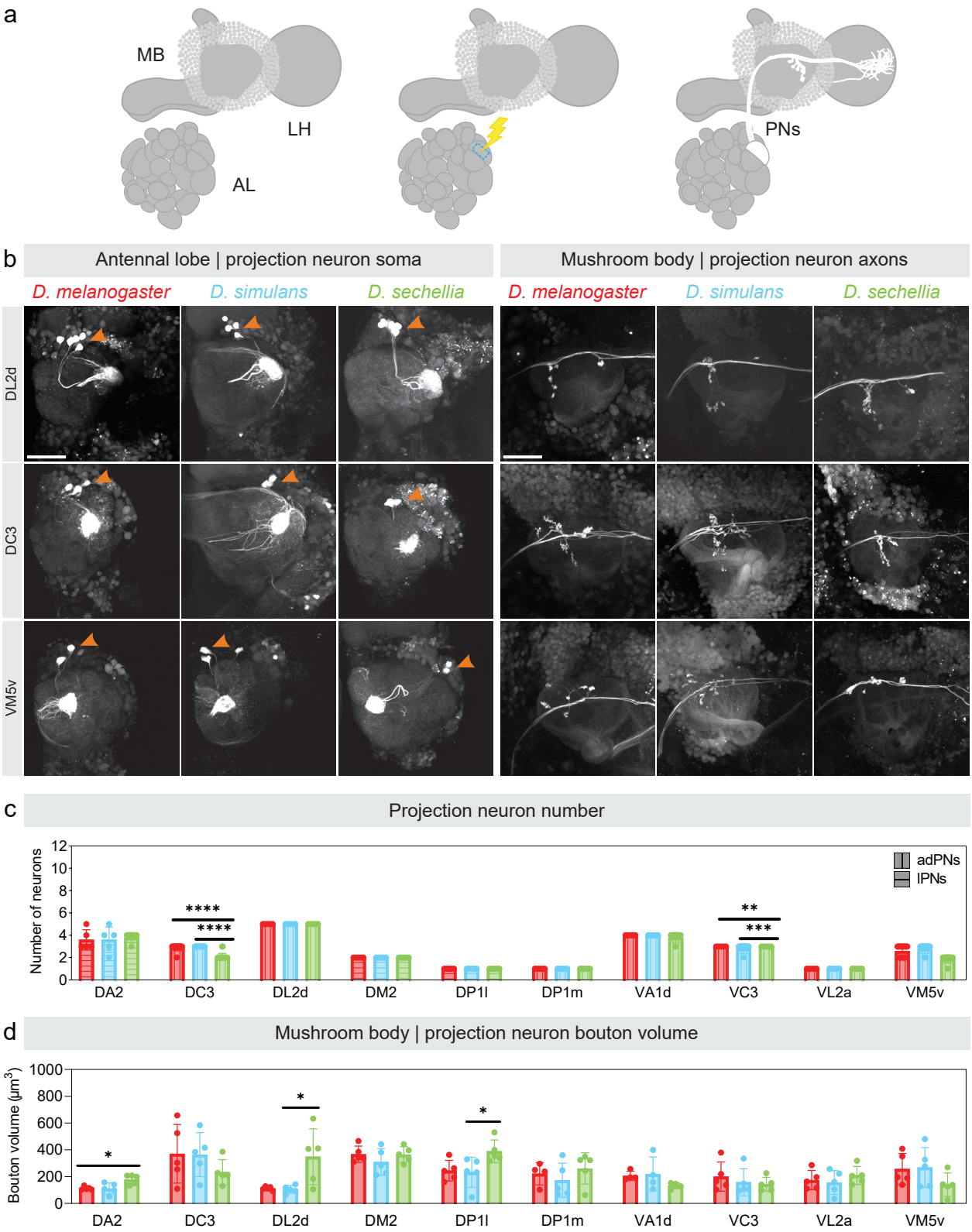
a
MB
LH
AL
PNs
b
Antennal lobe | projection neuron soma
Mushroom body | projection neuron axons
D. melanogaster
D. simulans
D. sechellia
D. melanogaster
D. simulans
D. sechellia
DL2d
DC3
VM5v
c
Projection neuron number
Number of neurons
adPNs
lPNs
****
****
**
***
DA2
DC3
DL2d
DM2
DP1l
DP1m
VA1d
VC3
VL2a
VM5v
d
Mushroom body | projection neuron bouton volume
Bouton volume (µm3)
*
*
*
DA2
DC3
DL2d
DM2
DP1l
DP1m
VA1d
VC3
VL2a
VM5v

Figure 3

Figure 3. Morphological features of the projection neurons innervating a given glomerulus in different *Drosophila* species. (a) Schematic depicting the technique used to photo-label the projection neurons innervating a given glomerulus: a glomerulus is used as a landmark for photo-labeling (blue dashed outline) and the projection neurons connected to the targeted glomerulus
635 are photo-labelled after successive rounds of photo-labeling. (b) The projection neurons innervating the DL2d (upper row), DC3 (middle row) and VM5v (lower row) glomeruli were photo-labeled in *D. melanogaster* (left column of each panel), *D. simulans* (middle column of each panel) and *D. sechellia* (right column of each panel). The cell bodies of these neurons (left panels) and the morphology of the axonal termini that these neurons extend in the mushroom body (right
640 panels) were imaged. Scale bar is 50 µm. (c-d) The number of photo-labeled neurons (c) and the volume of the presynaptic boutons these neurons form in the mushroom body (d) were quantified and compared across species (red: *D. melanogaster*; blue: *D. simulans*; green: *D. sechellia*). The statistical significance, or '*p*-value', was measured using the Mann-Whitney U test (*: *p*-value < 0.5, **: *p*-value < 0.01, ***: *p*-value < 0.001). See Table 1 for quantifications.
645

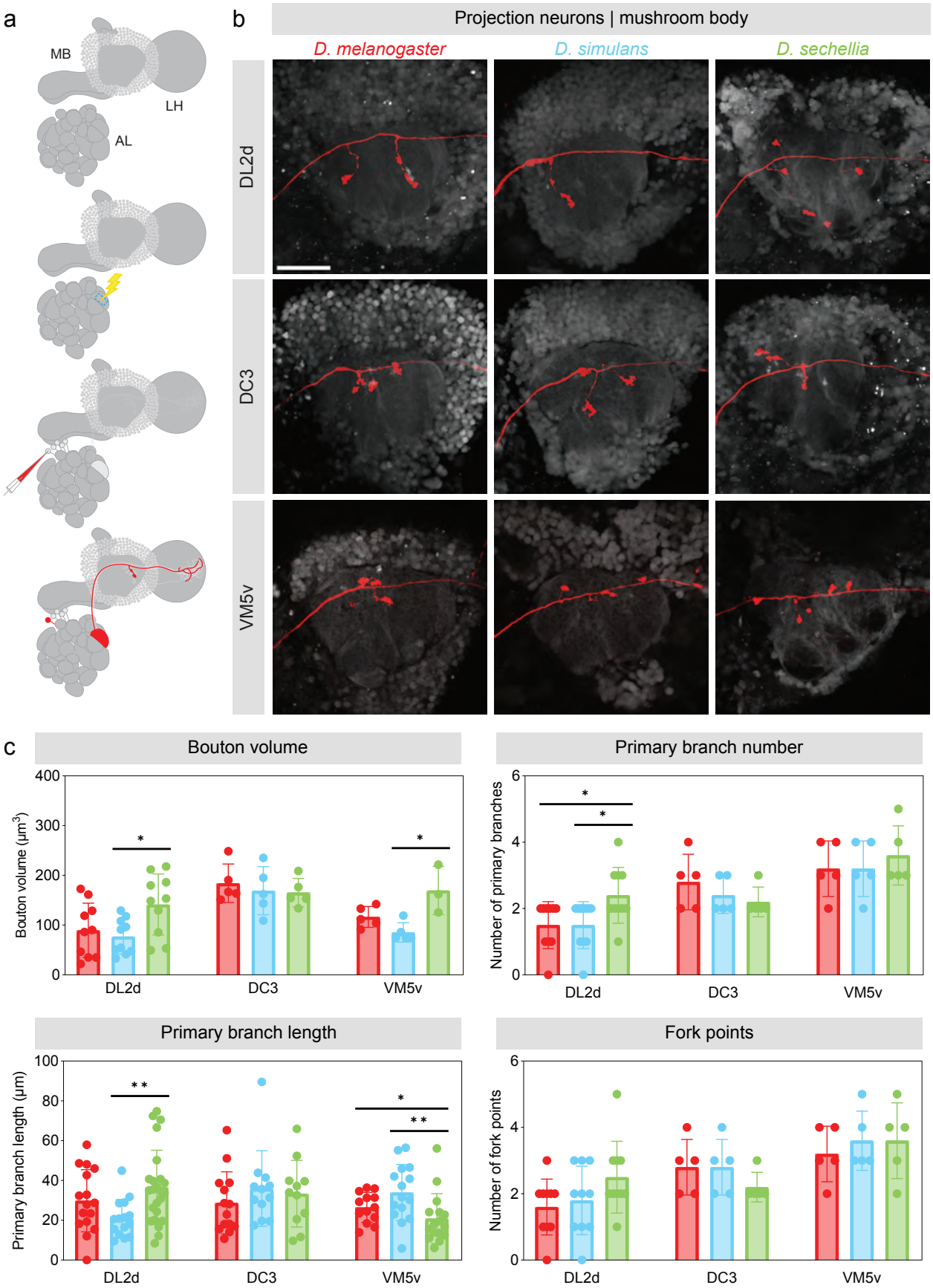
a
MB
LH
AL
b
Projection neurons | mushroom body
D. melanogaster
D. simulans
D. sechellia
DL2d
DC3
VM5v
c
Bouton volume
Bouton volume (μm³)
Primary branch number
Number of primary branches
Primary branch length
Primary branch length (μm)
Fork points
Number of fork points
DL2d
DC3
VM5v

Figure 4

Figure 4. Morphological features of individual projection neurons in different *Drosophila* species. (a) Schematic depicting the technique used to dye-label a projection neuron innervating
650 a given glomerulus: a glomerulus is used as a landmark for a first round of photo-labeling (blue dashed outline) during which the projection neurons connected to the targeted glomerulus are lightly photo-labelled; dye is electroporated in one of the photo-labeled projection neurons and a single projection neuron is dye-labeled. (b) A projection neuron innervating the DL2d (upper row), DC3 (middle row) and VM5v (lower row) glomeruli were dye-labeled in *D. melanogaster* (left
655 column of each panel), *D. simulans* (middle column of each panel) and *D. sechellia* (right column of each panel). The morphology of the axonal termini these neurons extend in the mushroom body were imaged. Scale bar is 50 μm. (c-d) Various morphological features displayed by projection neurons in the mushroom body were quantified and compared across species (red: *D. melanogaster*; blue: *D. simulans*; green: *D. sechellia*). The statistical significance, or '*p*-value',
660 was measured using the Mann-Whitney U test (*: *p*-value < 0.5, **: *p*-value < 0.01, ***: *p*-value < 0.001). See Extended Data Table 3 for quantifications.

Extended Data Table 1 | Comparison of glomerular volumes across species.

Glomerulus	Mean ± s.d. volume (μm^3)			*p* -values		
	D. melanogaster	*D. simulans*	*D. sechellia*	*Dmel vs Dsim*	*Dsim vs Dsec*	*Dmel* vs *Dsec*
D	2464 ± 40	1479 ± 186	2405 ± 131	0.1717	0.166161	0.72114
DA1	4391 ± 123	3379 ± 218	2766 ± 238	0.1717	0.166161	0.117068
DA2	1147 ± 62	1276 ± 200	1196 ± 123	0.751188	>0.999999	>0.999999
DA3	476 ± 10	455 ± 53	451 ± 56	0.751188	>0.999999	0.72114
DA4l	1133 ± 182	916 ± 71	837 ± 52	0.542211	0.490571	0.117068
DA4m	1097 ± 4668	1035 ± 110	814 ± 86	0.751188	0.303	0.228933
DC1	2530 ± 144	1433 ± 217	1249 ± 148	0.1717	0.490571	0.117068
DC2	1487 ± 178	1380 ± 152	904 ± 62	0.751188	0.166161	0.117068
DC3	1665 ± 172	1749 ± 201	1163 ± 89	0.751188	0.166161	0.117068
DC4	1702 ± 147	1270 ± 116	1050 ± 26	0.1717	0.166161	0.117068
DL1	2006 ± 232	1618 ± 297	1448 ± 103	0.542211	0.819477	0.117068
DL2d	1565 ± 334	2007 ± 185	3066 ± 296	0.303	0.166161	0.117068
DL2v	1712 ± 164	1381 ± 141	1798 ± 59	0.1717	0.166161	0.72114
DL3	1531 ± 213	1561 ± 158	931 ± 81	>0.999999	0.166161	0.117068
DL4	687 ± 47	1027 ± 96	1010 ± 90	0.1717	>0.999999	0.117068
DL5	1614 ± 50	1765 ± 195	1394 ± 13	0.751188	0.166161	0.117068
DM1	3408 ± 168	4238 ± 90	2057 ± 73	0.1717	0.166161	0.117068
DM2	3139 ± 227	3169 ± 227	4594 ± 127	0.751188	0.166161	0.117068
DM3	1846 ± 93	1542 ± 113	1053 ± 56	0.1717	0.166161	0.117068
DM4	3341 ± 64	2399 ± 130	724 ± 40	0.1717	0.166161	0.117068
DM5	1784 ± 194	1900 ± 164	968 ± 96	0.751188	0.166161	0.117068
DM6	1854 ± 42	1632 ± 134	2002 ± 137	0.303	0.166161	0.117068
DP1l	3269 ± 172	3118 ± 211	2173 ± 68	0.751188	0.166161	0.117068
DP1m	5117 ± 47	3399 ± 164	2465 ± 241	0.1717	0.166161	0.117068
V	3837 ± 194	3429 ± 126	2200 ± 146	0.1717	0.166161	0.117068
VA1d	3785 ± 148	1668 ± 126	2157 ± 194	0.1717	0.166161	0.117068
VA1v	5275 ± 160	3048 ± 330	2676 ± 187	0.1717	0.490571	0.117068
VA2	4204 ± 199	3474 ± 130	1987 ± 125	0.1717	0.166161	0.117068
VA3	1937 ± 120	1627 ± 233	894 ± 50	0.303	0.166161	0.117068
VA4	1894 ± 174	1244 ± 217	871 ± 124	0.1717	0.303	0.117068
VA5	1606 ± 220	1400 ± 170	811 ± 87	0.542211	0.166161	0.117068
VA6	2604 ± 38	1929 ± 107	1505 ± 115	0.1717	0.166161	0.117068
VA7l	1388 ± 80	1285 ± 291	963 ± 98	>0.999999	0.490571	0.117068
VA7m	1554 ± 144	783 ± 81	791 ± 105	0.1717	>0.999999	0.117068
VC1	1495 ± 214	1073 ± 66	816 ± 99	0.1717	0.166161	0.117068
VC2	1382 ± 97	1140 ± 176	918 ± 121	0.303	0.303	0.117068
VC3l	1911 ± 207	1912 ± 111	1265 ± 117	>0.999999	0.166161	0.117068
VC3m	1644 ± 187	1856 ± 253	2236 ± 180	0.542211	0.490571	0.117068
VC4	1456 ± 159	1053 ± 152	844 ± 105	0.1717	0.490571	0.117068
VC5	1408 ± 285	1238 ± 65	1294 ± 172	0.751188	>0.999999	0.72114
VL1	4319 ± 169	3062 ± 249	2503 ± 83	0.1717	0.166161	0.117068
VL2a	3222 ± 184	2014 ± 186	1954 ± 88	0.1717	>0.999999	0.117068
VL2p	2912 ± 278	1983 ± 180	2137 ± 181	0.1717	0.819477	0.117068
VM1	1397 ± 44	961 ± 93	1095 ± 109	0.1717	0.490571	0.117068
VM2	1505 ± 51	1869 ± 104	1225 ± 116	0.1717	0.166161	0.117068
VM3	1689 ± 135	2225 ± 193	1157 ± 114	0.1717	0.166161	0.117068
VM4	1862 ± 131	1476 ± 29	822 ± 57	0.1717	0.166161	0.117068
VM5d	905 ± 115	1773 ± 127	3793 ± 153	0.1717	0.166161	0.117068
VM5v	885 ± 112	1311 ± 140	1258 ± 75	0.1717	>0.999999	0.117068
VM7d	2006 ± 128	1139 ± 148	983 ± 138	0.1717	0.490571	0.117068
VM7v	2074 ± 65	1114 ± 123	766 ± 101	0.1717	0.166161	0.117068

665 **Extended Data Table 1. Comparison of glomerular volumes across species.** Individual glomeruli were reconstructed and their volumes were measured in *D. melanogaster*, *D. simulans* and *D. sechellia*. The statistical significance, or '*p*-value', measured when comparing glomerular volumes across species using the Mann-Whitney U test is reported. See Extended Data Figure 1 for antennal lobe reconstructions.

670

Extended Data Table 2 | Comparison of connectivity frequencies across species.

Projection neurons	Connectivity frequencies (%)				*p*-values			
	D. melanogaster ♂	*D. melanogaster* ♀	*D. simulans* ♀	*D. sechellia* ♀	*D. mel* ♂ vs *D. mel* ♀	*D. mel* ♀ vs *D. sim* ♀	*D. mel* ♀ vs *D. sec* ♀	*D. sec* ♀ vs *D. sim* ♀
D	1.62	2.32	2.86	1.52	0.425959605	0.4905764	0.223935288	0.038427193
DA1	4.58	4.06	3.55	3.65	0.778245101	0.883851349	0.459571107	0.652175845
DA2	0.30	0.58	0.55	0.00	0.685144443	1	0.05470851	0.05470851
DA3	0.74	0.44	0.14	0.61	0.723803923	0.623122645	1	0.373022311
DA4l	1.77	0.87	1.36	1.22	0.227128239	0.445158162	0.788185041	0.632869079
DA4m	0.44	0.73	0.41	2.13	0.723803923	0.723803923	0.059660897	0.01159878
DC1	3.25	3.34	3.27	1.98	1	1	0.05712051	0.039988316
DC2	1.77	1.89	3.00	1.98	1	0.156186533	1	0.080450785
DC3	3.10	4.50	4.91	1.37	0.180625798	0.592667752	0.000105671	6.18E-06
DC4	2.36	2.32	2.05	1.37	1	1	0.147838687	0.206892267
DL1	3.55	4.35	3.14	4.10	0.464853173	0.376551016	0.56886663	0.763680006
DL2d	1.48	1.02	0.68	3.19	0.621458754	0.770974186	0.010694533	0.002030026
DL2v	1.03	1.31	1.23	1.67	0.799595811	1	0.82097212	0.82097212
DL3	0.89	0.44	1.09	1.06	0.502847061	0.220084926	0.33984394	0.795466181
DL4	0.59	0.73	0.27	0.15	1	0.449002775	0.112650766	0.613468255
DL5	3.55	3.05	3.55	3.50	0.75204701	0.535045313	1	0.544441424
DM1	1.33	1.45	1.09	2.13	1	0.810237765	0.533357908	0.277753804
DM2	2.96	1.60	2.73	2.74	0.13365255	0.13365255	0.253777803	0.613857416
DM3	1.18	1.89	1.50	2.28	0.370388453	0.833788211	0.847166759	0.548846908
DM4	1.18	1.74	0.68	1.67	0.492339853	0.134934872	0.830944308	0.204291441
DM5	1.03	1.16	3.14	1.82	1	0.007926823	0.496514006	0.035486152
DM6	3.40	3.05	3.00	2.13	0.873268472	1	0.162789094	0.120351577
DP1l	1.18	0.44	0.95	3.19	0.220084926	0.337551088	0.000213936	0.010694533
DP1m	4.28	2.18	2.32	3.04	0.036854781	0.854131504	0.596532034	0.863436941
V	0.15	0.29	0.00	0.15	1	0.498753117	0.613468255	1
VA1d	2.80	5.08	3.14	2.13	0.027536162	0.1178755	0.000724388	0.087663066
VA1v	3.55	3.19	3.14	2.58	0.875676232	1	0.317509584	0.248227378
VA2	0.30	2.32	1.50	3.65	0.001031737	0.425959605	0.318251718	0.050561389
VA3	2.36	3.19	2.73	3.50	0.394264773	0.870681446	1	0.872283898
VA4	0.89	1.16	0.68	0.76	0.786786471	0.574666345	0.405371318	1
VA5	2.95	2.90	3.41	4.10	1	0.527282216	0.439439778	1
VA6	3.40	4.06	2.59	2.43	0.549227132	0.213996386	0.038444931	0.486360178
VA7l	2.36	1.16	1.50	3.04	0.139211456	0.639451754	0.031730484	0.139574504
VA7m	1.48	1.16	2.18	0.46	0.810237765	0.139211456	0.131061437	0.001633421
VC1	1.77	1.60	1.77	0.91	1	0.833788211	0.217840514	0.099602749
VC2	1.62	1.16	2.32	1.06	0.639451754	0.096786652	0.795466181	0.033801205
VC3	4.43	2.90	4.77	2.13	0.173313664	0.041431671	0.282487997	0.000724388
VC4	2.07	1.74	2.46	0.61	0.839757049	0.342810912	0.040115307	0.001600336
VL1	0.44	0.44	0.14	0.61	1	0.623122645	1	0.373022311
VL2a	3.69	4.21	1.36	3.34	0.661130386	0.002068546	0.232488704	0.044418781
VL2p	2.07	3.05	2.05	1.98	0.288407238	0.382727077	0.151082094	0.696176189
VM1	1.33	2.03	2.73	3.50	0.39084755	0.370369465	0.227325455	0.872283898
VM2	0.59	0.73	1.50	2.28	1	0.200868828	0.038263936	0.548846908
VM3	1.48	0.58	0.82	2.43	0.171890629	0.75079102	0.010561	0.048459961
VM4	2.81	1.74	0.95	3.34	0.261734954	0.347514666	0.11141934	0.006767902
VM5d	2.81	2.76	1.64	1.82	1	0.261734954	0.19035229	1
VM5v	4.73	3.63	5.05	1.82	0.391120027	0.128272711	0.016285553	5.83E-05
VM7d	2.36	3.05	3.96	1.98	0.4905764	0.290035725	0.151082094	0.005537156
VM7v	0.00	0.44	0.14	0.91	0.248129676	0.623122645	0.504685649	0.12292742

Extended Data Table 2. Comparison of connectivity frequencies across species. The frequencies at which projection neurons innervating a given glomerulus are connected to Kenyon cells were measured based on the number of connections detected in the connectivity matrices shown in Figure 1d. The statistical significance, or '*p*-value', for each glomerulus was obtained by using a binomial test to compare the connection frequency of each glomerulus to the mean frequency; red text indicates *p*-value < 0.01.

Extended Data Table 3 | Morphological features of dye-labeled projection neurons across species.

Morphological features	DL2d projection neurons			DC3 projection neurons			VM5v projection neurons		
	D. melanogaster	***D. simulans***	***D. sechellia***	***D. melanogaster***	***D. simulans***	***D. sechellia***	***D. melanogaster***	***D. simulans***	***D. sechellia***
Bouton cluster volume (μm^3)	89.65 ± 51.87	77.09 ± 33.41	141.54 ± 58.24	184.15 ± 34.60	169.01 ± 43.23	165.36 ± 25.56	116.45 ± 18.68	85.38 ± 17.48	169.73 ± 39.67
Primary axonal branch number	1 ± 0.70	2 ± 0.70	3 ± 1.27	2 ± 0.40	2 ± 0.49	2 ± 0.75	3 ± 0.70	4 ± 0.50	4 ± 1.20
Primary axonal branch length (μm)	29.84 ± 15.14	21 ± 9.18	35.08 ± 19.31	28.76 ± 15.10	35.96 ± 18.17	33.37 ± 15.99	26.46 ± 7.17	33.92 ± 13.68	20.84 ± 12.13
Axonal fork points	2 ± 0.80	2 ± 0.98	3 ± 1.02	3 ± 0.75	3 ± 0.75	2 ± 0.40	3 ± 0.75	4 ± 0.80	4 ± 1.02

Extended Data Table 3. Morphological features of dye-labeled projection neurons across species. Morphological features of individual DC3, DL2d and VM5v projection neurons — namely the presynaptic bouton volume, the number of axonal primary branches and their length, and the number of forks they form in the mushroom body — were measured and compared across species (n = 5 for DC3 neurons, n = 10 for DL2d neurons and n = 5 for VM5d neurons). The statistical significance (p-value) of the differences between species for each of the morphological features was measured with the Mann-Whitney U Test. See Figure 4b for representative images of each projection neuron type.

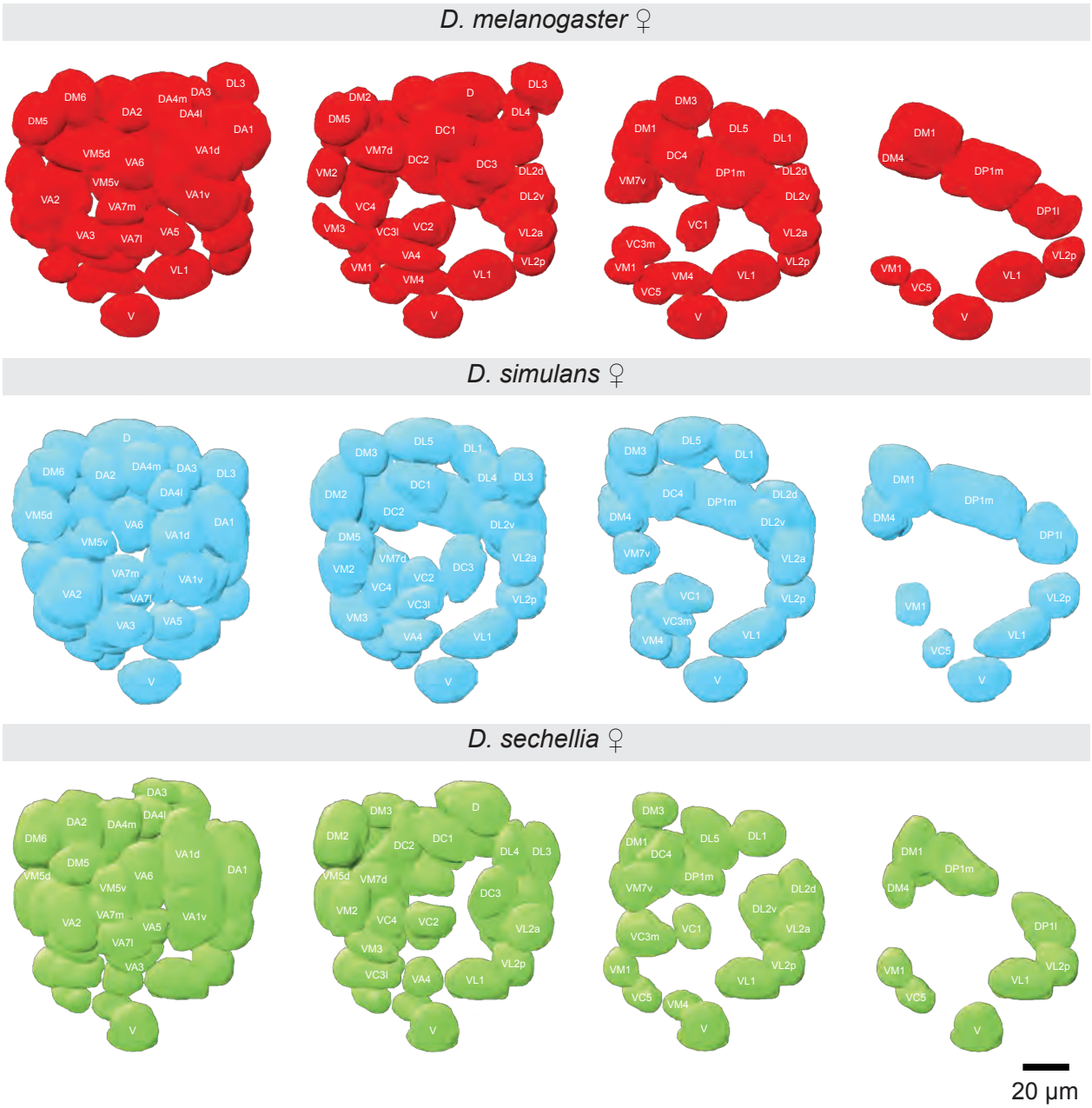

Extended Data Figure 1

Extended Data Figure 1. Antennal lobe reconstructions in different species. The brains of two- or three-day old *D. melanogaster* (red), *D. simulans* (blue), and *D. sechellia* (green) female
695 flies were fixed, immuno-stained (using the nc82 monoclonal antibody against Bruchpilot) and imaged (*n* = 3 for each species). The glomeruli forming the antennal lobe were individually reconstructed and identified based on shape and location. Three different planes are shown for each reconstruction. Scale bar is 20 μm. See Extended Data Table 1 for quantifications.

700

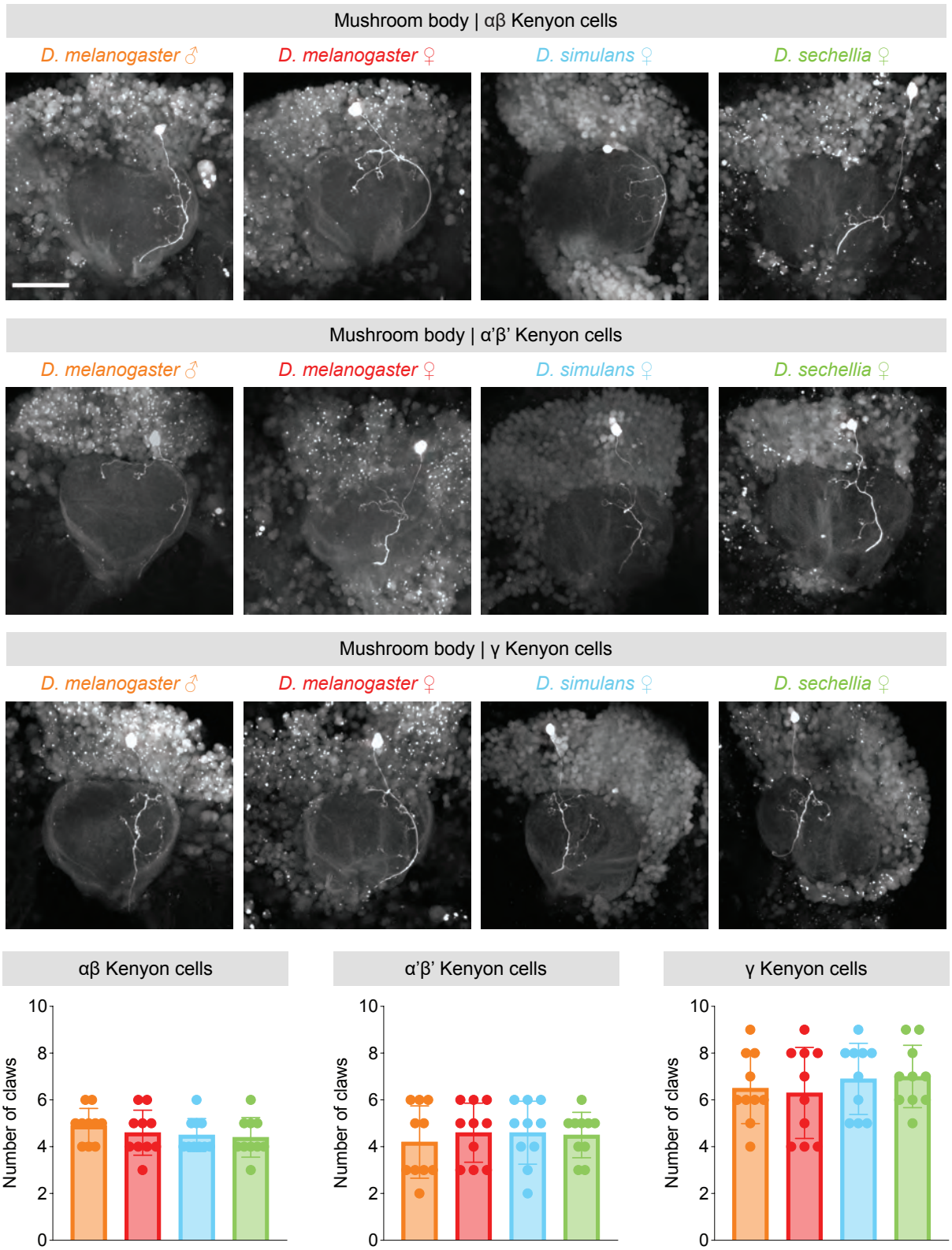

Extended Data Figure 2

Extended Data Figure 2. Morphological features of Kenyon cells across species. Individual α/β (top panels), α'/β' (middle panels), and γ Kenyon cells (bottom panels) were photo-labeled in *D. melanogaster*, *D. simulans*, and *D. sechellia* flies, and the postsynaptic terminals formed by these neurons in the mushroom body calyx — called 'claws' — were imaged (orange: *D. melanogaster* males; red: *D. melanogaster* females; blue: *D. simulans*; green: *D. sechellia*). Scale bar is 50 μm. The total number of claws per Kenyon cell were counted (n = 10). The statistical significance, or 'p-value', was measured for each type of Kenyon cell using the Mann-Whitney U test but none of the values were found to be significantly different.

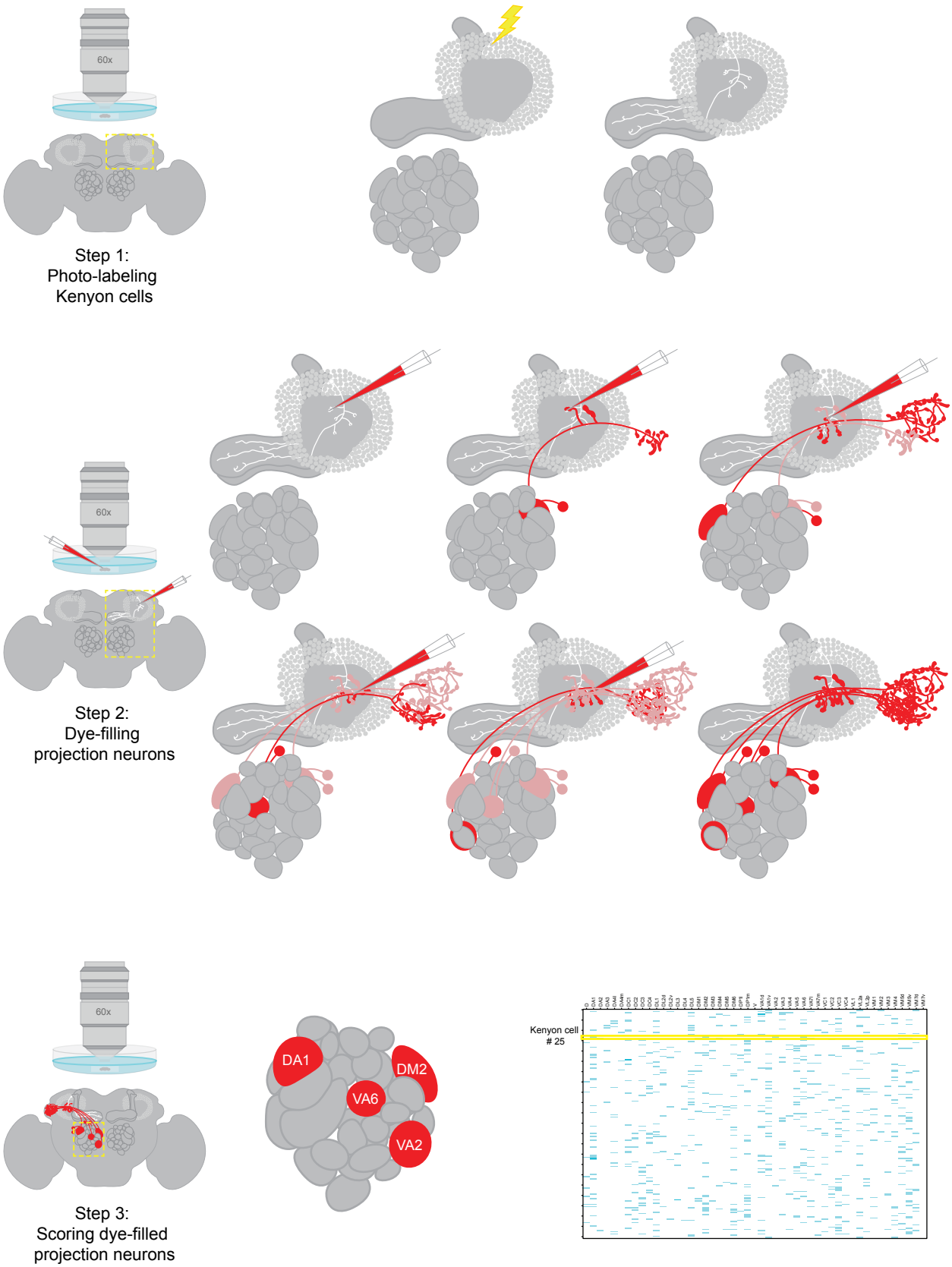

Extended Data Figure 3

Extended Data Figure 3. Mapping technique. Step 1 — Photo-labeling Kenyon cells: The brain of a fly carrying the *nSynaptobrevin-GAL4* and *UAS-photoactivatable-GFP* transgenes is
715 dissected and imaged using 2-photon microscopy; a randomly selected Kenyon cell is targeted with high energy light (yellow) such that the photoactivatable-GFP molecules is converted only in that cell; the converted photoactivatable-GFP molecules rapidly diffuse in the Kenyon cell revealing its entire morphology (white). Step 2 — Dye-filling projection neurons: A post-synaptic terminal — or 'claw' — is targeted with an electrode filled with Texas Red dextran dye, and,
720 following a short current pulse, the dye is electroporated into the projection neuron connected to that claw; this procedure can be repeated with other claws. Step 3 — Scoring dye-filled projection neurons: The identity of the dye-labeled projection neurons connected to the photo-labeled Kenyon cell can be revealed by visualizing the antennal lobe. The glomerular inputs of a given Kenyon cell — in this example the DA1, DM2, VA2 and VA6 glomeruli — is reported as a line in
725 a connectivity matrix; each matrix reports the inputs identified for 200 Kenyon cells.

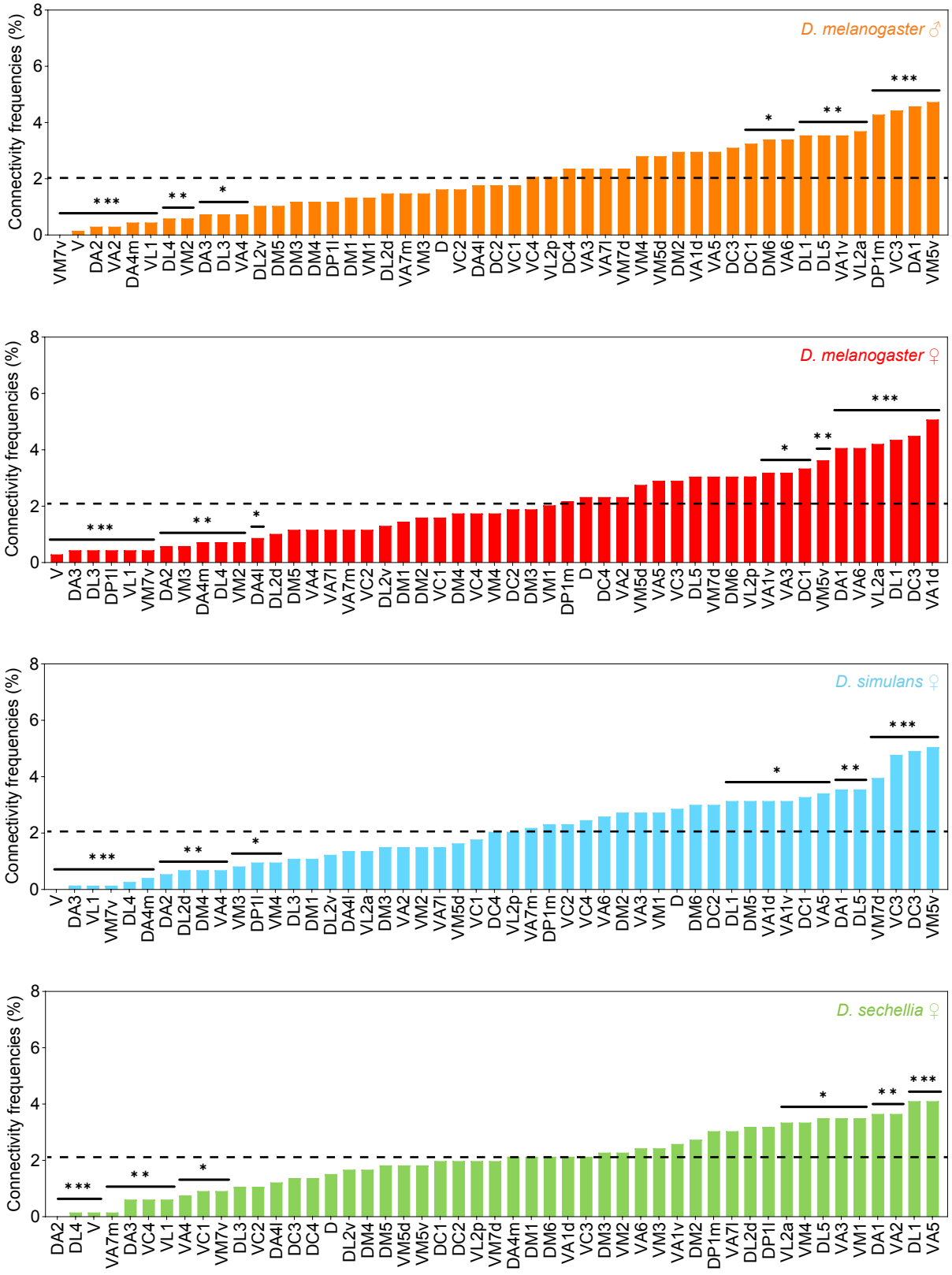

Extended Data Figure 4

Extended Data Figure 4. Non-uniform distribution of connectivity frequencies. The
730 frequencies at which individual glomeruli are connected to Kenyon cells was determined based on the number of connections detected between projection neurons and Kenyon cells in each connectivity matrix reported in Figure 1d (orange: *D. melanogaster* males; red: *D. melanogaster* females; blue: *D. simulans*; green: *D. sechellia*). Glomeruli that are significantly under- or overrepresented are labeled with asterisks (*: *p*-value < 0.5, **: *p*-value < 0.01, ***: *p*-value <
735 0.001).

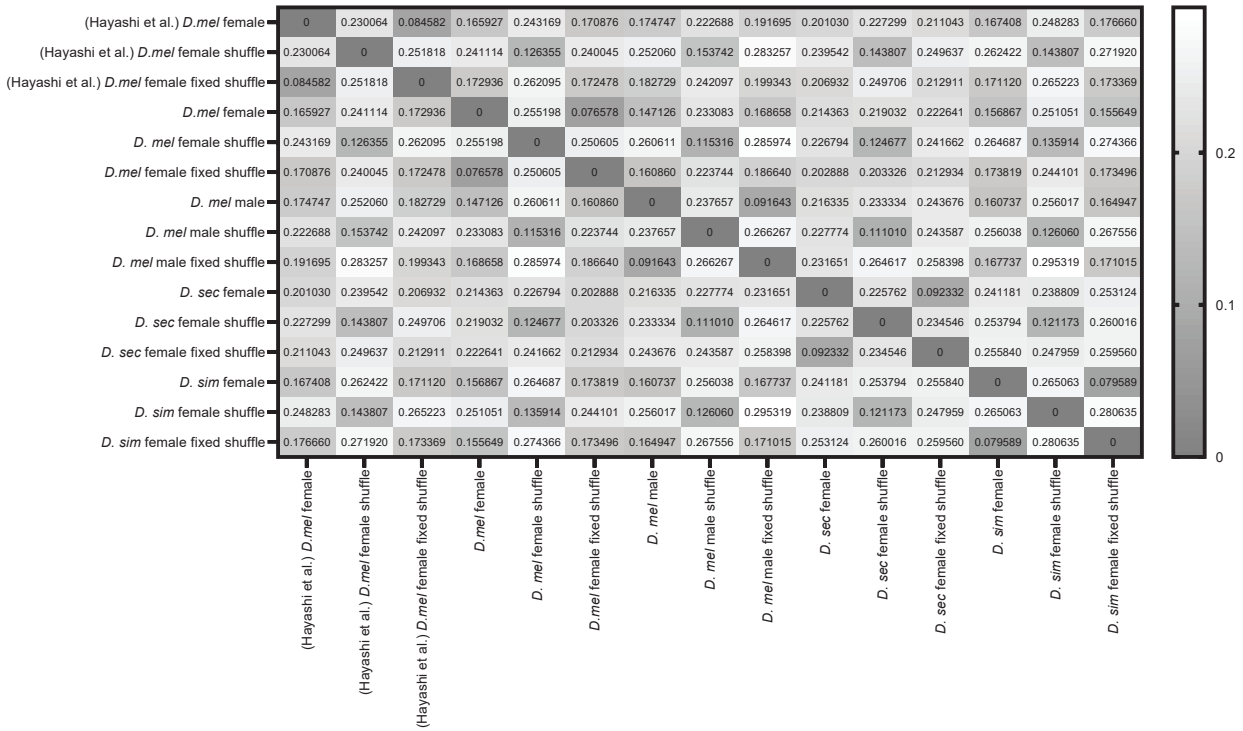

Extended Data Figure 5

Extended Data Figure 5. Jensen-Shannon distances. The Jensen-Shannon distances were measured by comparing the distributions in connectivity frequencies observed in the experimental matrices — this study or a previous study[28] — and the uniform shuffle and biased shuffle matrices; distances are reported as a heat map. The color bar denotes the length of the distances measured.

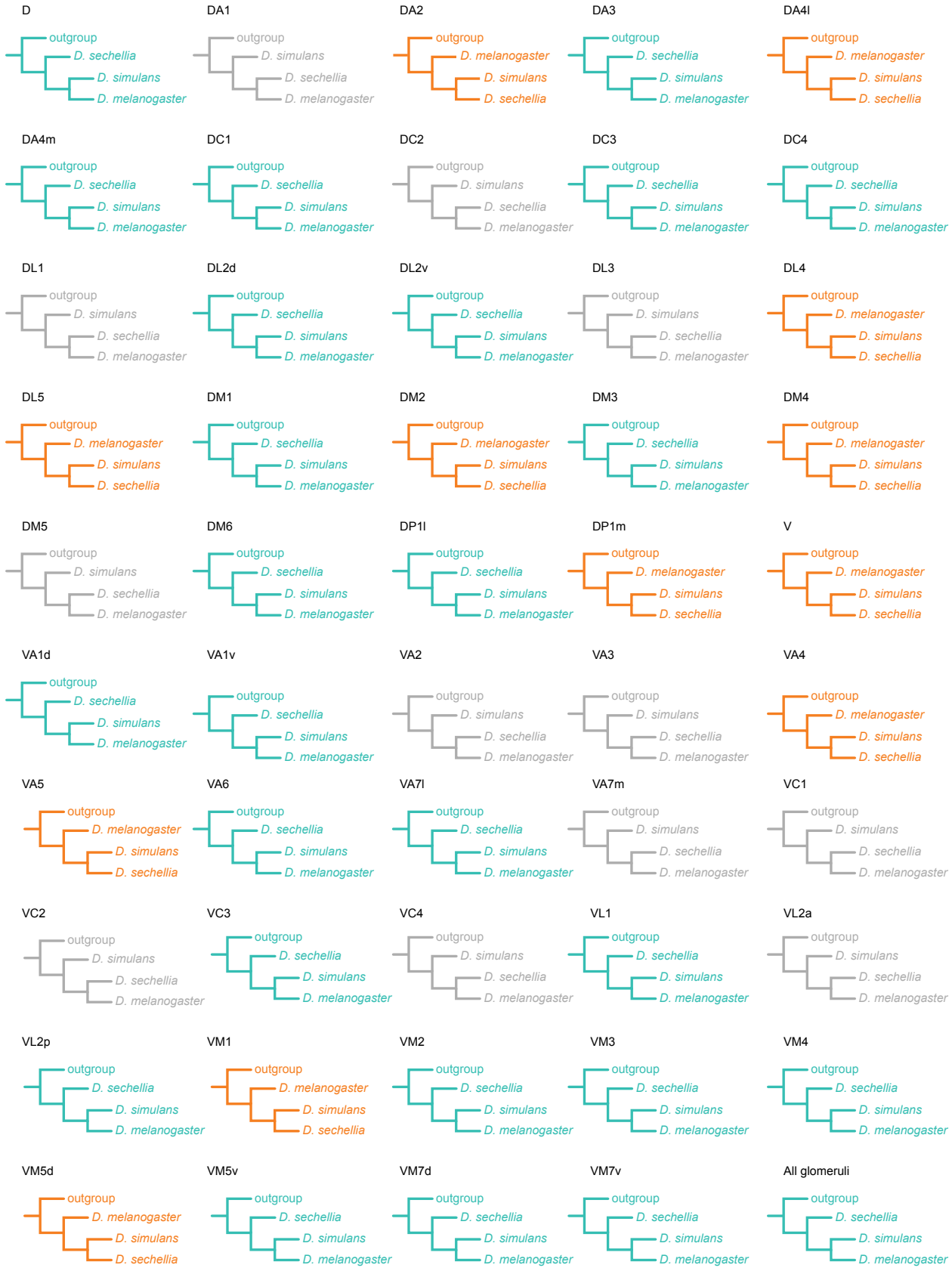

Extended Data Figure 6

Extended Data Figure 6. Similarity trees built using connectivity frequencies. Similarity trees were generated with the Tree analysis Using New Technology (TNT) software. The connectivity frequencies of a given glomerulus observed in the species of interest were used as traits; a value
750 of 100/49 or 2.04816 was used for the glomeruli forming the outgroup. Trees were generated either for individual glomeruli or for all glomeruli; trees either follow the known phylogenetic relationships (orange), the ecological relationships (aqua) or neither (grey).

Extended Data Figure 7

Extended Data Figure 7. Similarity trees built using receptor sequences. Similarity trees were generated with the Tree analysis Using New Technology (TNT) software. The cDNA sequence of the receptor gene associated with a given glomerulus was used as traits; the cDNA sequences of *D. yakuba* (Gr10a, Ir31a, Ir76a, Or9a, Or22a, Or23a, Or46a, Or49a, Or65a, OR67a,
760 Or67d, Or69a, Or82a, Or85a, Or85b, Or85d, Or88a, Or92a, Or98a) or *D. elegans* (Gr21a, Ir64a, Ir75a, Ir75b, Ir75c, Ir75d, Ir84a, Ir92a, Or2a, Or7a, Or13a, Or19a, Or33c, Or35a, Or42a, Or42b, Or43a, Or43b, Or47a, Or47b, Or49b, Or56a, Or59b, Or59c, Or67b, Or67c, Or71a, Or83c) were used as the outgroup. Trees were generated either for individual glomeruli or for all glomeruli; all trees follow the known phylogenetic relationships (orange).

765

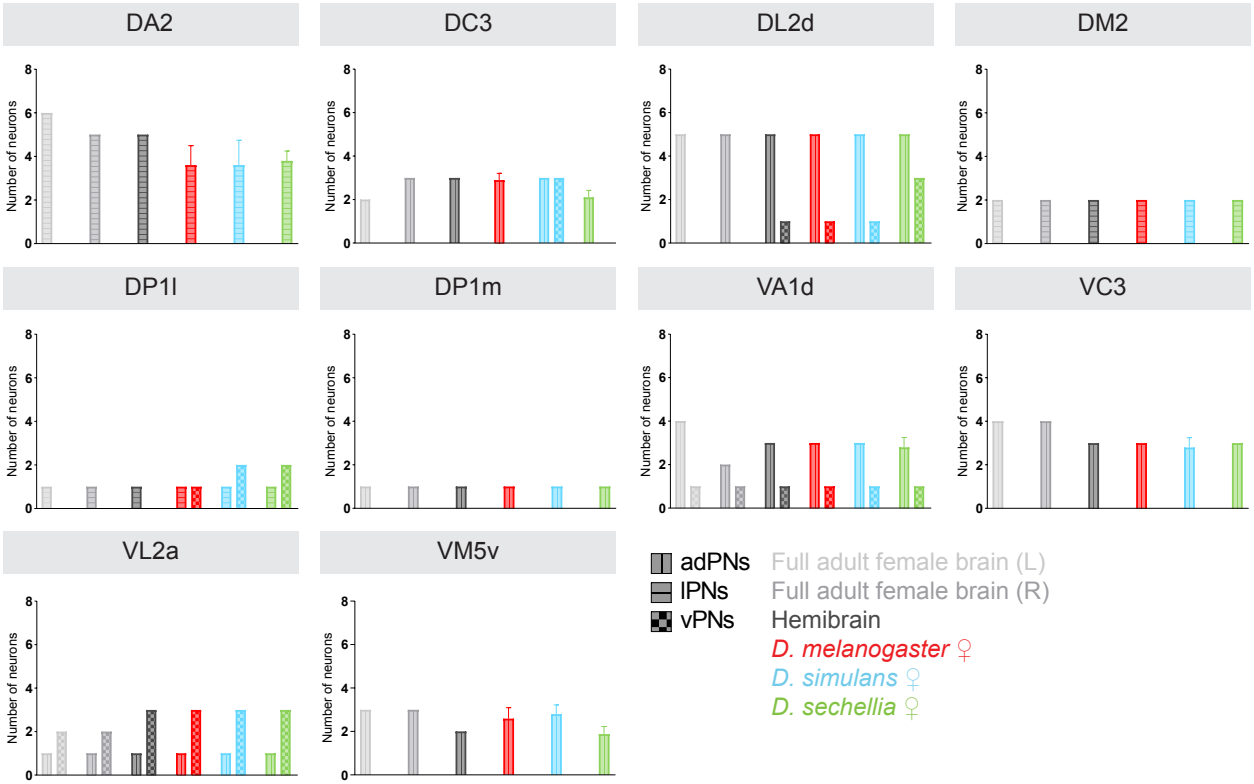

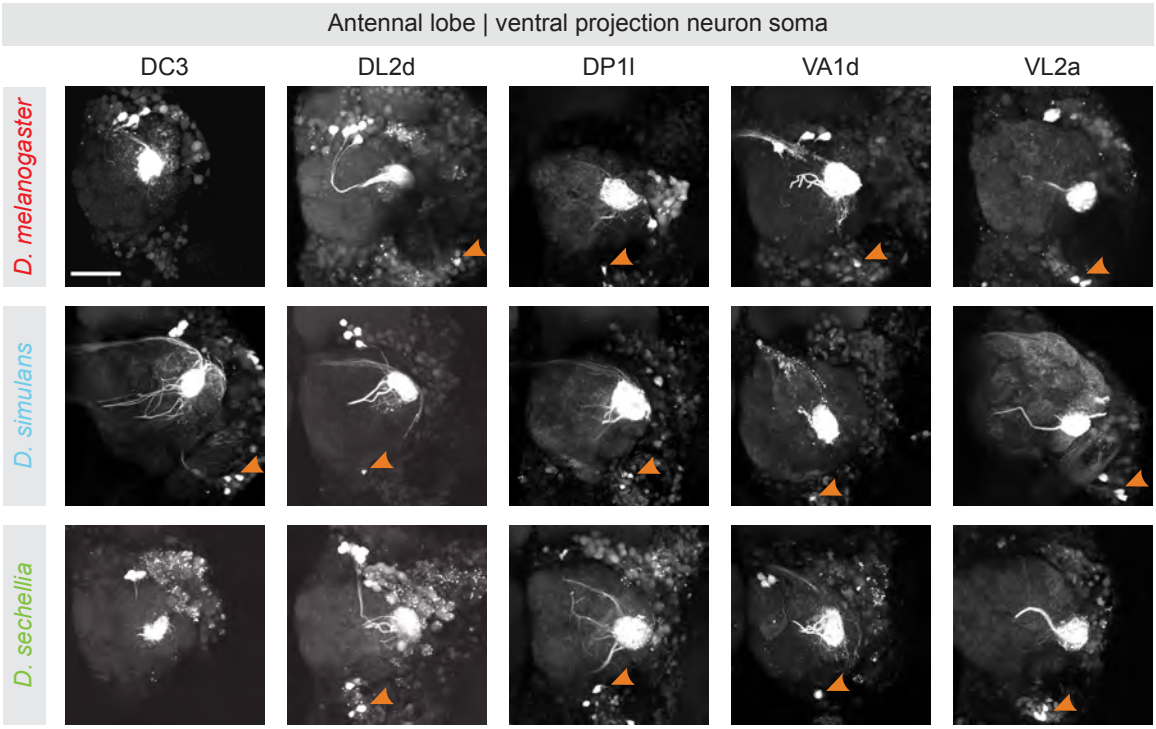

Extended Data Figure 8

Extended Data Figure 8. Number of projection neurons per glomerulus. The number of projection neurons associated with the DA2, DC3, DL2d, DM2, DP1l, DP1m, VA1d, VC3, VL2a,
770 and VM5v glomeruli — divided by types (vertical lines: adPNs; horizontal lines: lPNS; checkers: vPNs) — were compared across species based on the data sets collected in this study and the available *D. melanogaster* connectomes[22] (light grey: FAFB connectome, left side; medium grey: FAFB connectome, right side; dark grey: hemibrain connectome). The cell bodies of the photo-labeled projection neurons (DC3, DL2d, DP1l, VA1d, and VL2a) that are located in the ventral
775 cluster were imaged (orange arrows). Scale bar is 50 μm.

Projection neurons showing significant shifts in connectivity frequencies

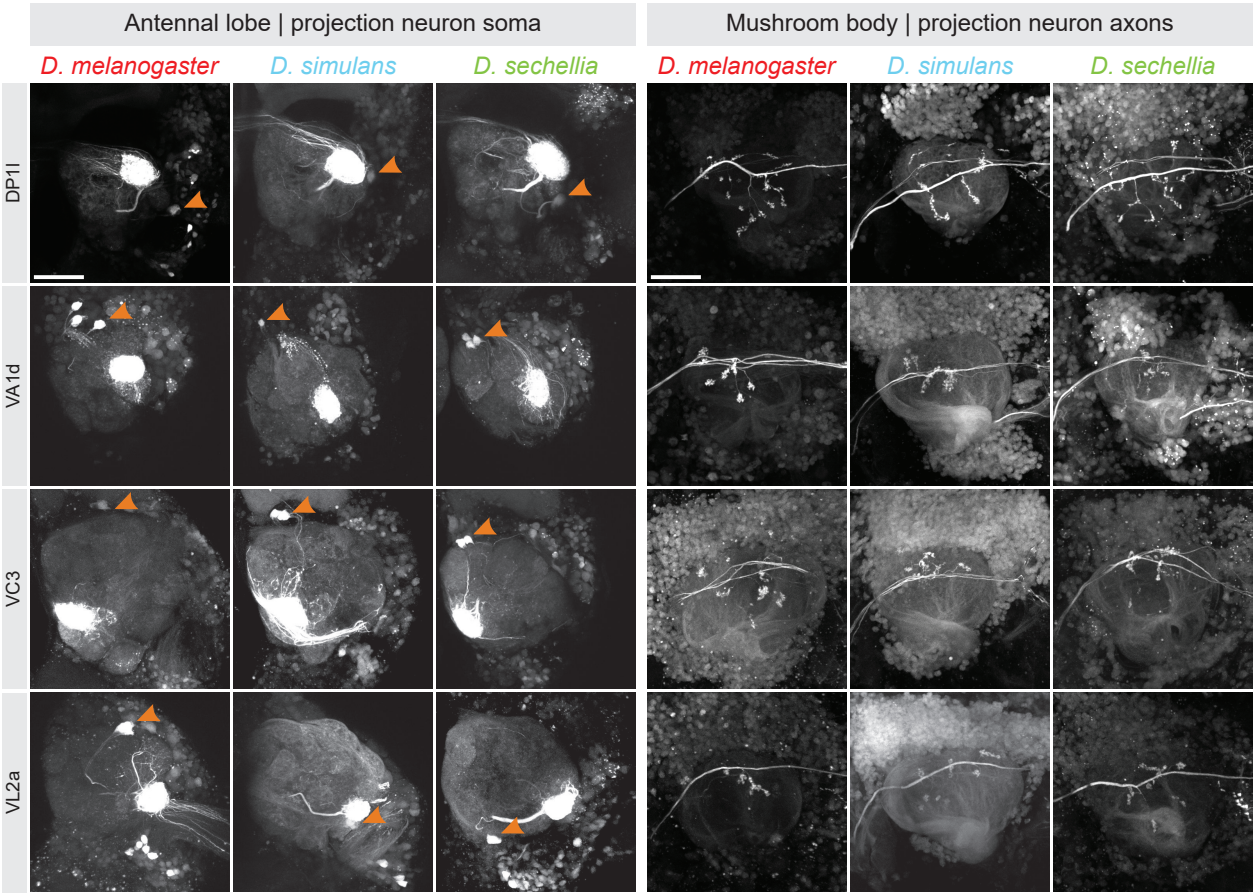

Projection neurons without significant shifts in connectivity frequencies

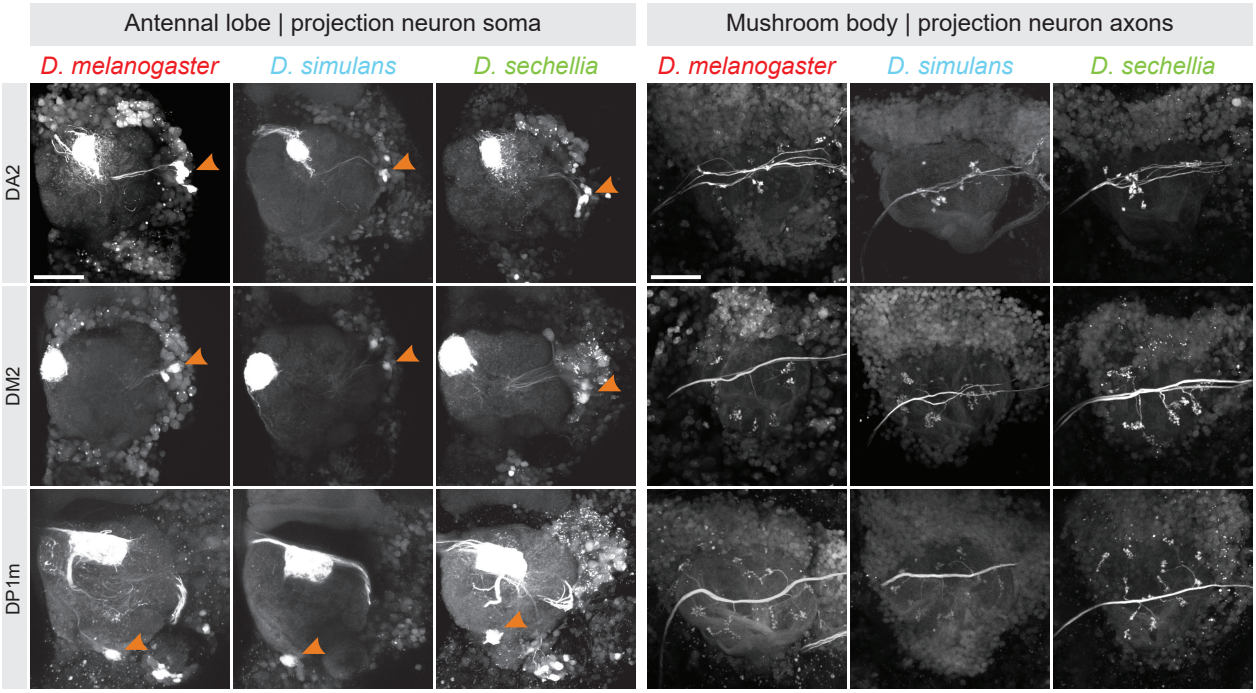

Extended Data Figure 9

Extended Data Figure 9. Morphological features of projection neurons across species.
780 Projection neurons showing significant shifts in connectivity frequencies (DP1l, VA1d, VC3 and VL2a) were analyzed as well as projection neurons showing no such shifts (DA2, DM2 and DP1m). Projection neurons were photo-labeled in *D. melanogaster*, *D. simulans* and *D. sechellia*; the location of the cell bodies of the photo-labeled neurons relative to the antennal lobe (orange arrows) and the morphology of the axonal termini that these neurons extend in the mushroom
785 body were imaged. Scale bar is 50 μm. See Table 1 for quantifications.

METHODS

790 **Fly stocks and husbandry**

Flies were reared under standard conditions (25°C, 60% humidity) in incubators that maintain a 12 h light:12h dark cycle (Percival Scientific Inc, Cat#DR36VL); *Drosophila melanogaster* and *Drosophila simulans* flies were reared on standard cornmeal agar medium, whereas *Drosophila*
795 *sechellia* flies were reared on standard cornmeal agar medium that was supplemented with noni juice (Healing Noni). The stocks used and their sources were as follows: *D. melanogaster*: *w*^{1118}*;;;* (Bloomington Stock Center, 5905), *yw;[N-Synaptobrevin-GAL4]*$^{2.1}$*;;* (J. Simpson, University of California, Santa Barbara)[23] and *y*^{1}*,w*^{1118}*;[10xUAS-IVS-Syn21-mC3PA-GFP-p10]*^{attP40}*;;* (Axel laboratory, Columbia University)[23]; *D. sechellia*: *w[N-Synaptobrevin-GAL4, w*]3P3-RFP-DEL;;;*
800 and *w[UAS-C3PA-GFP, w*]3P3-RFP-DELA;;;* (Benton laboratory, University of Lausanne)[16]; *D.* simulans: *attp*^{2176} y^{1}*w*^{1}*; pBac [3P3-EYFP-DEL, attp];;* and *attp*^{2178} *y*^{1}*w*^{1}*;; pBac [3P3-EYFP-DEL, attp];* (Stern laboratory, Janelia Farm Research Campus)[38].

Reconstructing antennal lobes

805

Antennal lobes were reconstructed from confocal images of immuno-stained brains. The brains of flies were dissected at room temperature in a phosphate buffered saline solution or PBS (Sigma-Aldrich, P5493), fixed in 2% paraformaldehyde (Electron Microscopy Sciences, 15710) for either 45 min (*D. melanogaster*) or 35 min (*D. simulans* and *D. sechellia*) at room temperature,
810 washed five times in PBST (PBS with 1x Triton, Sigma-Aldrich, T8787) at room temperature, blocked with 5% goat Serum (Jackson ImmunoResearch Laboratories) in PBST for 30 min at room temperature, and incubated in a solution that contained the primary antibody (1:20 in 5% Goat Serum/PBST, Developmental Studies Hybridoma Bank, nc82, AB_2314866) at 4°C overnight. On the following day, brains were washed four times in PBST and incubated in a
815 solution that contained the secondary antibody (1:500 in 5% Goat Serum/PBST, Thermal Fisher, goat anti-mouse Alexa Fluor 488, AB_2576217) at 4°C overnight. On the following day, brains were washed four times in PBST and mounted on a slide (Fisher Scientific, 12-550-143) using the mounting media VECTASHIELD (Vector Laboratories Inc., H-1000). Immuno-stained brains were imaged using an LSM 880 confocal microscope (Zeiss). Each antennal lobe was
820 reconstructed from a confocal image using the segmentation software Amira (FEI Visualization Sciences Group, version 2020.3.1). Individual glomeruli were reconstructed via manual

segmentation: boundaries were demarcated by hand and interpolated. Glomeruli were assigned identities according to their position based on the available anatomical maps and the *Drosophila melanogaster* hemibrain connectome v1.2.1[13,14,29,39]. Glomerular volumes were calculated from
825 the reconstructed voxel size, and the sum of those volumes were used to calculate whole antennal lobe volumes. We identified a total of 51 glomeruli in the antennal lobe reconstructions but only 49 in the mapping experiments used to generate the connectivity matrices. This is because VC3 is split into two glomeruli — VC3m and VC3l — in the reconstructions but when scoring matrices, we could not distinguish VC3m from VC3l.

830

Photo-labeling projection neurons and Kenyon cells

Neurons were photo-labeled based on a previously published protocol[40]. In short, brains were dissected in saline (108 mM NaCl, 5 mM KCl, 5 mM HEPES, 5 mM Trehalose, 10 mM Sucrose,
835 1 mM NaH_2PO_4, 4 mM $NaHCO_3$, 2 mM $CaCl_2$, 4 mM $MgCl_2$, pH≈7.3), treated for 1 min with 2 mg/ml collagenase (Sigma-Aldrich) and mounted on a piece of SYLGARD placed at the bottom of a Petri dish. Each brain was either mounted with its anterior side facing upward (for photo-labeling projection neurons) or with its posterior side facing upward (for photo-labeling Kenyon cells). The photo-labeling and image acquisition steps were performed using a two-photon laser
840 scanning microscope (Bruker, Ultima) with an ultrafast Chameleon Ti:Sapphire laser (Coherent) modulated by Pockels Cells (Conotopics). During the photo-labeling step, the laser was tuned to 710 nm and about 5 to 30 mW of laser power was used; during the image acquisition step, the laser was tuned to 925 nm and about 1 to 14 mW of laser power was used. Both power values were measured behind the objective lens. A 60X water-immersion objective lens (Olympus) was
845 used for both photo-labeling and image acquisition. A GaAsP detector (Hamamatsu Photonics) was used for measuring green fluorescence. Photo-labeling was performed by drawing a region of interest — on average 1.0 x 1.0 µm — either in the center of the targeted glomerulus (for labeling projection neurons) or in the center of the soma (for labeling Kenyon cells). Photo-labeling projection neurons: Photoactivation was achieved through two to four cycles of exposure to 710-
850 nm laser light, during which each pixel was scanned four times, with 25 repetitions per cycle, and 15 min rest period between each cycle. Image acquisition was performed with the laser tuned to 925 nm at a resolution of 512 by 512 pixels with a pixel size of 0.39 µm and a pixel dwell time of 4 µs; each pixel was scanned twice. A minimum of five samples per species were analyzed for each type of projection neuron. Photo-labeling Kenyon cells: Photoactivation was achieved
855 through three to five single scans with the laser tuned to 710 nm, during which each pixel was

scanned eight times. Before image acquisition, a 10 min rest period was implemented to allow diffusion of the photoactivated fluorophore within the neuron. Image acquisition was performed at a resolution of 512 by 512 pixels with a pixel size of 0.39 μm and a pixel dwell time of 4 μs; each pixel was scanned 2 times.

860

Mapping Kenyon cell input connections using dye electroporation

The projection neurons connecting to a photo-labeled Kenyon cell were identified based on previously published protocols[25,28]. In short, electrodes were made by pulling borosilicate glass
865 pipette with filament (Sutter Instruments, BF100-50-10) to a resistance of 9-11 MΩ, fire-polished using a micro-forge (Narishige) to narrow their opening, and backfilled with 100mg/ml 3000-Da Texas-dextran dye (Thermo-Fisher, D3328). Under the guidance of a two-photon microscope (Bruker, Ultima), an electrode was centered into the post-synaptic terminal — or 'claw' — of a photo-labeled Kenyon cell using a motorized micromanipulator (Sutter Instruments). Short current
870 pulses (each 10-50 V in amplitude and 0.5 millisecond long) were applied until the projection neuron connecting to the targeted Kenyon cell claw was visible. Not all the projection neurons connecting to a given Kenyon cells were dye-filled but on average 4 ± 1 of the claws formed by a given Kenyon cell were dye-filled. An image of the antennal lobe was acquired at the end of the procedure. Dye-labeled glomeruli were identified based on their shape, position and the location
875 of their soma as defined in the available anatomical maps and the *Drosophila melanogaster* hemibrain connectome v1.2.1[13,14,29,39].

Dye-labeling individual projection neurons

880 Individual projection neurons were dye-labeled using a previously published protocol[16,41]. The cell body of the projection neuron of interest was first identified by lightly photo-labeling all the projection neurons innervating a given glomerulus by performing a single cycle of exposure to 710 nm light. After a rest period of 10 min, an unpolished electrode filled with Texas Red dextran dye was attached to the cell body of one of the photo-labeled projection neurons, and the dye
885 was electroporated into the neuron using short current pulses; each pulse was 10 to 30 V in amplitude and 0.5 millisecond long. A resting period of about 30 min allowed the dye to diffuse throughout the neuron. Image acquisition was performed at a resolution of 512 by 512 pixels with a pixel size of 0.39 μm and a pixel dwell time of 4 μs; each pixel was scanned 2 times. A minimum of five samples per species were analyzed for each type of projection neuron.

890

Quantifying morphological features of projection neurons

Representative images of projection neurons were projected at maximal intensity using the ImageJ/Fiji software[42] (National Institutes of Health). Projection neurons were counted based on
895 the number of photo-labeled cell bodies observed in the anterior or lateral or ventral clusters of the antennal lobe. Primary branches were defined as processes that emerge from the main axonal projection that traverses the calyx of the mushroom body. The length of the branches formed by a projection neuron and the number of forks were quantified using the 'Simple Neurite Tracer' plugin for ImageJ/Fiji software, while the surface area of the axonal arbors in the mushroom body
900 calyx and lateral horn was calculated using the 'ROI Manager' and 'Measure' features of this software[43] (National Institutes of Health). Total projection neuron bouton volume for a given sample was measured using Fluorender (University of Utah Scientific Computing and Imaging Institute; version 2.26.2[49,50]): boutons were traced using the 'Paint Brush' function. To distinguish boutons from the background, the 'Edge Detect' parameter was kept on and the 'Edge STR' was
905 fixed at 0.505, while the selection threshold was adjusted to different values depending on signal intensity[44]. The 'Physical Size' value of the traced boutons was reported as total bouton volume.

Similarity trees

910 Similarity trees, which were built using either the connectivity frequencies of glomeruli or the coding sequences of olfactory receptors, were generated using the 'Traditional Search' option in the Tree Analysis Using New Technologies (TNT) program (v.1.5)[45]. The cDNA sequences of *D. melanogaster* olfactory receptors were used as queries in BLASTN searches of *D. simulans* and *D. sechellia* cDNA sequences using the default settings of BLAST+v.2.13.0; *D. elegans* and *D.*
915 *yakuba* cDNA sequences were used as outgroups[46]. Genomic regions were annotated using the Gnomon gene prediction method[47]. Coding sequence alignment of olfactory receptors was generated with MUSCLE, and the evolutionary history was determined with the 'Maximum Likelihood' method[48,49]. Sequences were edited manually to obtain the final alignments.

920 **Statistical analyses**

For the statistical analyses of the data shown in Table 1, Figure 3, 4, Extended Data Table 1, 3 and Extended Data Figure 3, 4 and 9, *p*-values were computed using the Mann-Whitney U test;

statistical significance is indicated as $p < 0.05$ (*), $p < 0.01$ (**) and $p < 0.001$ (***). For the statistical analyses of the data shown in Figure 2 and Extended Data Table 2, *p*-values were computed using the Fisher's exact test; to control for false positives, *p*-values were adjusted with a false discovery rate of 10% using a Benjamini-Hochberg procedure.

METHODS REFERENCES

1. Striedter, G. F. & Northcutt, R. G. *Brains Through Time*. (Oxford University Press, 2019). doi:10.1093/oso/9780195125689.001.0001.
2. Striedter, G. F. *Principles of brain evolution. Principles of brain evolution.* (Sinauer Associates, 2005).
3. Strausfeld. *Arthropod Brains*. (2011).
4. Tosches, M. A. From Cell Types to an Integrated Understanding of Brain Evolution: The Case of the Cerebral Cortex. *Annu Rev Cell Dev Biol* **37**, 495–517 (2021).
5. Roberts, R. J. v, Pop, S. & Prieto-Godino, L. L. Evolution of central neural circuits: state of the art and perspectives. *Nat Rev Neurosci* **23**, 725–743 (2022).
6. Markow, T. A. The secret lives of Drosophila flies. *Elife* **4**, (2015).
7. Drosophila 12 Genomes Consortium *et al.* Evolution of genes and genomes on the Drosophila phylogeny. *Nature* **450**, 203–18 (2007).
8. Sturtevant, A. H. A New Species Closely Resembling Drosophila Melanogaster. *Psyche (Camb Mass)* **26**, 153–155 (1919).
9. Tsacas, L. & Bächli, G. Drosophila sechellia. n. sp., huitieme espece du sous-groupe melanogaster des iles Seychelles (Diptera, Drosophilidae). *Rev. Fr. Entomol 3* 146–150 (1981).
10. R'Kha, S., Capy, P. & David, J. R. Host-plant specialization in the Drosophila melanogaster species complex: a physiological, behavioral, and genetical analysis. *Proceedings of the National Academy of Sciences* **88**, 1835–1839 (1991).
11. Auer, T. O., Shahandeh, M. P. & Benton, R. *Drosophila sechellia* : A Genetic Model for Behavioral Evolution and Neuroecology. *Annu Rev Genet* **55**, 527–554 (2021).
12. Lachaise, D. & Silvain, J.-F. How Two Afrotropical Endemics Made Two Cosmopolitan Human Commensals: the Drosophila Melanogaster–D. Simulans Palaeogeographic Riddle. *Genetica* **120**, 17–39 (2004).
13. Couto, A., Alenius, M. & Dickson, B. J. Molecular, anatomical, and functional organization of the Drosophila olfactory system. *Current Biology* **15**, 1535–1547 (2005).
14. Fishilevich, E. & Vosshall, L. B. Genetic and functional subdivision of the Drosophila antennal lobe. *Current Biology* **15**, 1548–1553 (2005).
15. McBride, C. S. & Arguello, J. R. Five Drosophila Genomes Reveal Nonneutral Evolution and the Signature of Host Specialization in the Chemoreceptor Superfamily. *Genetics* **177**, 1395–1416 (2007).
16. Auer, T. O. *et al.* Olfactory receptor and circuit evolution promote host specialization. *Nature* **579**, 402–408 (2020).

17. Stensmyr, M. C., Dekker, T. & Hansson, B. S. Evolution of the olfactory code in the *Drosophila melanogaster* subgroup. *Proc R Soc Lond B Biol Sci* **270**, 2333–2340 (2003).
18. Dekker, T., Ibba, I., Siju, K. P., Stensmyr, M. C. & Hansson, B. S. Olfactory shifts parallel superspecialism for toxic fruit in Drosophila melanogaster sibling, D. sechellia. *Current Biology* **16**, 101–109 (2006).
19. Ibba, I., Angioy, A. M., Hansson, B. S. & Dekker, T. Macroglomeruli for fruit odors change blend preference in Drosophila. *Naturwissenschaften* **97**, 1059–1066 (2010).
20. Prieto-Godino, L. L. *et al.* Evolution of Acid-Sensing Olfactory Circuits in Drosophilids. *Neuron* **93**, 661-676.e6 (2017).
21. Jefferis, G. S. X. E. *et al.* Comprehensive Maps of Drosophila Higher Olfactory Centers: Spatially Segregated Fruit and Pheromone Representation. *Cell* **128**, 1187–1203 (2007).
22. Schlegel, P. *et al.* Information flow, cell types and stereotypy in a full olfactory connectome. *Elife* **10**, (2021).
23. Aso, Y. *et al.* The neuronal architecture of the mushroom body provides a logic for associative learning. *Elife* **3**, (2014).
24. Li, F. *et al.* The connectome of the adult Drosophila mushroom body provides insights into function. *Elife* **9**, (2020).
25. Caron, S. J. C., Ruta, V., Abbott, L. F. & Axel, R. Random convergence of olfactory inputs in the Drosophila mushroom body. *Nature* **497**, 113–117 (2013).
26. Gruntman, E. & Turner, G. C. Integration of the olfactory code across dendritic claws of single mushroom body neurons. *Nat Neurosci* **16**, 1821–1829 (2013).
27. Zheng, Z. *et al.* Structured sampling of olfactory input by the fly mushroom body. *Current Biology* **32**, 3334-3349.e6 (2022).
28. Hayashi, T. T. *et al.* Mushroom body input connections form independently of sensory activity in Drosophila melanogaster. *Current Biology* **32**, 4000-4012.e5 (2022).
29. Grabe, V. *et al.* Elucidating the Neuronal Architecture of Olfactory Glomeruli in the Drosophila Antennal Lobe Resource Elucidating the Neuronal Architecture of Olfactory Glomeruli in the Drosophila Antennal Lobe. 3401–3413 (2016).
30. Hallem, E. A. & Carlson, J. R. Coding of Odors by a Receptor Repertoire. *Cell* **125**, 143–160 (2006).
31. Ronderos, D. S., Lin, C.-C., Potter, C. J. & Smith, D. P. Farnesol-Detecting Olfactory Neurons in Drosophila. *Journal of Neuroscience* **34**, 3959–3968 (2014).
32. Münch, D. & Galizia, C. G. DoOR 2.0 - Comprehensive Mapping of Drosophila melanogaster Odorant Responses. *Sci Rep* **6**, 21841 (2016).
33. Dweck, H. K. M. *et al.* Pheromones mediating copulation and attraction in *Drosophila*. *Proceedings of the National Academy of Sciences* **112**, (2015).
34. Zhao, Z. & McBride, C. S. Evolution of olfactory circuits in insects. *Journal of Comparative Physiology A* **206**, 353–367 (2020).
35. Luo, S. X., Axel, R. & Abbott, L. F. Generating sparse and selective third-order responses in the olfactory system of the fly. *Proceedings of the National Academy of Sciences* **107**, 10713–10718 (2010).
36. Stevens, C. F. What the fly's nose tells the fly's brain. *Proceedings of the National Academy of Sciences* **112**, 9460–9465 (2015).

37. Litwin-Kumar, A., Harris, K. D., Axel, R., Sompolinsky, H. & Abbott, L. F. Optimal Degrees of Synaptic Connectivity. *Neuron* **93**, 1153-1164.e7 (2017).
38. Stern, D. L. *et al.* Genetic and Transgenic Reagents for *Drosophila simulans* , *D. mauritiana* , *D. yakuba* , *D. santomea* , and *D. virilis*. *G3 Genes|Genomes|Genetics* **7**, 1339–1347 (2017).
39. Scheffer, L. K. *et al.* A connectome and analysis of the adult Drosophila central brain. *Elife* **9**, (2020).
40. Li, J., Ellis, K. E. & Caron, S. J. C. Photo-labeling neurons in the Drosophila brain. *STAR Protoc* **2**, 100381 (2021).
41. Ruta, V. *et al.* A dimorphic pheromone circuit in Drosophila from sensory input to descending output. *Nature* **468**, 686–690 (2010).
42. Schindelin, J. *et al.* Fiji: an open-source platform for biological-image analysis. *Nat Methods* **9**, 676–682 (2012).
43. Longair, M. H., Baker, D. A. & Armstrong, J. D. Simple Neurite Tracer: open source software for reconstruction, visualization and analysis of neuronal processes. *Bioinformatics* **27**, 2453–2454 (2011).
44. Wan, Y. *et al.* FluoRender: joint freehand segmentation and visualization for many-channel fluorescence data analysis. *BMC Bioinformatics* **18**, 280 (2017).
45. Goloboff, P. A., Farris, J. S. & Nixon, K. C. TNT, a free program for phylogenetic analysis. *Cladistics* **24**, 774–786 (2008).
46. Camacho, C. *et al.* BLAST+: architecture and applications. *BMC Bioinformatics* **10**, 421 (2009).
47. Souvorov, A. *et al.* Gnomon – NCBI eukaryotic gene prediction tool. Preprint at (2012).
48. Jones, D. T., Taylor, W. R. & Thornton, J. M. The rapid generation of mutation data matrices from protein sequences. *Bioinformatics* **8**, 275–282 (1992).
49. Edgar, R. C. MUSCLE: multiple sequence alignment with high accuracy and high throughput. *Nucleic Acids Res* **32**, 1792–1797 (2004).